International Journal of Secondary Metabolite
2026, Vol. 13, No. 2, 452–476
https://doi.org/10.21448/ijsm.1693171
journal homepage: https://dergipark.org.tr/en/pub/ijsm
Research Article

Isolation, characterization, and docking analysis of endophytic Aspergillus ochraceus NRRL398 metabolites from Eclipta prostrata (L.) L. *targeting acetylcholinesterase inhibition*

Vaishali Maruti Todkar[1*], Prasanna Vasantrao Habbu[1], Venkatrao Hanumantrao Kulkarni[1], Shrinivas Dattatraya Joshi[1], Smita Daniel Madagundi[1]

[1]Department of Pharmacognosy, SET's College of Pharmacy, S.R. Nagar, Dharwad-580002, Karnataka, India.

ARTICLE HISTORY

Received: May 6, 2025
Accepted: Feb. 1, 2026

KEYWORDS

Acetylcholinesterase inhibitory activity,
Aspergillus ochraceus,
Eclipta prostrata,
Endophytic fungi *in-silico*.

Abstract: *Eclipta prostrata* (False Daisy) is widely acknowledged in traditional medicine for its neuroprotective properties, primarily due to its abundant flavonoids and coumestans. However, the chemical and pharmacological potential of its associated endophytic fungi remains underexplored. In this study, we report for the first time the isolation of *Aspergillus ochraceus* NRRL398 as an endophyte from *E. prostrata*, and the subsequent isolation and characterization of nine bioactive secondary metabolites from its n-butanol fraction (EPSF-1-NB). Notably, this is the first report of Apigenin and Luteolin being produced by this fungal endophyte, highlighting its unprecedented biosynthetic capability. The isolated compounds comprising two triterpenoids, one phytosterol, two coumestan derivatives, and four flavonoids were structurally elucidated using advanced chromatographic and spectroscopic techniques. In-silico molecular docking against acetylcholinesterase (AChE, PDB ID: 1QTI) using SYBYL-X 2.0 software revealed that Apigenin and Luteolin exhibited the strongest binding affinities with C-scores of 6.93 and 6.88, respectively, outperforming other compounds such as Wedelolactone (5.48), dimethylwedelolactone (5.05), and sterol/triterpenoid constituents. This study provides novel insight into the metabolic versatility of *A. ochraceus* as an endophyte of *E. prostrata*, and identifies Apigenin and Luteolin as promising AChE inhibitors of fungal origin. These findings open new avenues for exploring fungal endophytes as untapped sources of neuroprotective agents and warrant further *in-vitro* and *in-vivo* validation.

INTRODUCTION

Recent advancements in drug discovery have increasingly emphasized the potential of bioactive metabolites derived from endophytic microorganisms, particularly fungi. Endophytes, microorganisms that reside asymptomatically within plant tissues, are emerging as prolific producers of structurally diverse secondary metabolites with significant pharmacological activities. These microbial products often mimic or share structural similarity with compounds naturally synthesized by their host plants, a phenomenon attributed to horizontal gene transfer and co-evolutionary adaptation (Li *et al.*, 1998; Ptak *et al.*, 2022; Strobel *et al.*, 2002). This structural resemblance underscores the biochemical versatility of endophytic fungi and their

*Corresponding Author: Vaishali Maruti TODKAR vaishalimalabade@gmail.com Department of Pharmacognosy, SET's College of Pharmacy, S.R. Nagar, Dharwad-580002, Karnataka, India

The copyright of the published article belongs to its author under CC BY 4.0 license. To view a copy of this licence, visit http://creativecommons.org/licenses/by/4.0/

e-ISSN: 2148-6905

importance in the field of natural product-based drug discovery. Fungal endophytes have attracted substantial attention due to their ecological diversity and capacity to generate compounds exhibiting a wide range of biological activities. Numerous reports have documented their antibacterial (Verma *et al*., 2009), antifungal (Hashem *et al.*, 2022), anticancer (Garyali *et al*., 2013), antioxidant (Yadav *et al.,* 2014), and antiviral (Zhang *et al.,* 2011) properties. Furthermore, certain fungal metabolites have demonstrated hepatoprotective, anti-inflammatory, and neuroprotective or nootropic effects (Kodoli *et al.,* 2021; Wen-Xia *et al.,* 2020), positioning endophytic fungi as valuable resources in the search for therapeutic agents against chronic and degenerative diseases.

Among medicinal plants recognized for their diverse therapeutic applications, *Eclipta prostrata* (L.) L. (commonly known as Bhringaraj or False Daisy) occupies a prominent position in traditional medicine systems such as Ayurveda, Siddha, and Traditional Chinese Medicine. Traditionally used to manage liver disorders, skin ailments, and neurological conditions, this plant is phytochemically rich in flavonoids, coumestans, phenolic acids, and triterpenoids, many of which contribute to its established antioxidant and neuroprotective properties (Rafif *et al.,* 2022; Silalahi *et al.,* 2022). Given this bioactive profile, *E. prostrata* serves as a promising host for isolating endophytes with potential neuroactive effects.

A previously published study (Todkar *et al.,* 2024) reported the isolation and molecular characterization of *Aspergillus ochraceus* NRRL398 from the healthy tissues of *E. prostrata*. Preliminary phytochemical screening of its crude extract and solvent fractions revealed that the n-butanol fraction (EPSF-1-NB) exhibited strong acetylcholinesterase (AChE) inhibitory activity *in vitro*. The inhibition of AChE is a well-established therapeutic mechanism for enhancing cholinergic neurotransmission in neurodegenerative diseases such as Alzheimer's disease (AD), where cholinergic deficits are a hallmark pathological feature. By preventing the breakdown of acetylcholine at synaptic junctions, AChE inhibitors improve cognitive function and delay the progression of symptoms in AD patients.

Given the promising *in vitro* activity, the current study focuses on the isolation, purification, and structural characterization of the active metabolites present in the EPSF-1-NB fraction of *A. ochraceus* NRRL398. The purified compounds were characterized using spectroscopic techniques, including Nuclear Magnetic Resonance (NMR) and Mass Spectrometry (MS). To complement the experimental findings and gain molecular-level insights into the binding interactions, in-silico molecular docking studies were performed using SYBYL-X 2.0 software**.** Molecular docking is a widely used computational approach in rational drug design, enabling the prediction of ligand–receptor binding interactions, affinities, and conformational stability. In this study, docking simulations were carried out using the crystal structure of acetylcholinesterase (PDB ID: 1QTI)**,** which represents the enzyme derived from *Torpedo californica* complexed with the reference inhibitor donepezil (E2020)**.** The choice of *T. californica* AChE is supported by its high sequence and active site homology with human AChE, combined with its historical utility in structural and inhibition studies due to the abundance of AChE in its electric organ, facilitating crystallization and analysis.

The combined use of classical phytochemical analysis and computational modeling in this investigation provides a comprehensive approach to exploring the AChE inhibitory potential of fungal endophyte-derived metabolites. This integrative strategy not only aids in the identification of lead compounds but also advances the understanding of their possible mechanisms of interaction at the molecular level, thereby contributing to the development of novel agents for managing neurodegenerative diseases.

MATERIAL and METHODS

The materials used in this study included Essae DS-450 and Wensar electronic balances for weighing the endophytic fungal fraction (EPSF-1-NB). The experiment employed a range of general laboratory equipment, including an electric water bath, a sonicator, an autoclave, and a hot air oven (Quality Instruments and Equipment). A Desaga Sarstedt-Gruppe UV cabinet was

used to observe TLC plates at 254 nanometre. Adsorption chromatography was executed using a separation column fitted with a glass stopcock and filled with silica gel stationary phase. and eluted with solvents like Pet ether, ethyl acetate, and chloroform. The rotary evaporator used was an Equitron Roteva. For spectroscopic analysis, a Shimadzu IR-Affinity Fourier Transform InfraRed Spectrophotometer with ATR, a Bruker advanced II 400 NMR Spectrometer, and a Waters Q TOF Micromass were utilized. The SYBYL-X 2.0 software (Tripos Inc.) and Surflex-Dock program were used for molecular docking (Gasteiger *et al.*, 1980; Joshi *et al*., 2014). The symbiotic fungus *Aspergillus ochraceus* NRRL398 was extracted from *Eclipta prostrata* and identified using DNA extraction, PCR amplification with ITS primers, sequencing, and BLAST analysis. Potato Dextrose Broth (PDB) was used as the fermentation medium for growing the fungus.

This study aims to isolate, characterize, and evaluate the acetylcholinesterase inhibitory potential of secondary metabolites derived from EPSF-1-NB through in-silico molecular docking analysis.

Isolation of Endophytic Fungi

Freshly harvested and shade-dried twigs, including the foliage and stalks of *Eclipta prostrata*, were collected from Tadakad village, located near Dharwad, Karnataka. The collected plant material was authenticated by a taxonomist from the Department of Botany, Karnataka Science College, Dharwad. Following authentication, a voucher specimen (SETCPD/Ph.cog/Herb/2022/01) was prepared and deposited in the Pharmacognosy division of the College of Pharmacy, Dharwad, under the aegis of Soniya Education Trust (SET).

The authenticated botanical specimens were thoroughly cleaned under running tap water to eliminate adhering dust and debris, followed by air-drying at room temperature. Subsequently, the leaves and stems were carefully separated before initiating the sterilization process. Surface sterilization involved sequential treatment: immersion in a 4% bleach solution for 5 minutes, followed by 70% ethanol for 1 minute, and finally rinsing with sterile distilled water for 1 minute. This sterilization cycle was repeated two to three times to ensure thorough decontamination.

To further isolate endophytes, selected surface-sterilized fragments were aseptically crushed in an alcohol-flamed mortar with distilled water to form suspensions, which were then subjected to serial dilutions. Both the sterilized plant fragments and aliquots of the diluted suspensions were inoculated onto sterile potato dextrose agar (PDA) plates supplemented with 150 mg/L streptomycin to suppress bacterial growth. The plates were incubated at 23–25°C for 7–14 days. Emerging fungal colonies were observed, isolated, and purified based on their distinct morphological characteristics. From this process, three genuine endophytic fungal strains designated EPLF-1, EPLF-2, and EPSF-1, associated with *Eclipta prostrata* were successfully identified and selected for further study (Wiyakrutta *et al*., 2004; Silva *et al*., 2005).

Molecular Identification of Endophytic Fungi

Genomic DNA of the endophytic fungus *Aspergillus ochraceus* NRRL398 was extracted using standard protocols involving cell lysis at 68°C for 30 minutes (Doty *et al*., 2005). Ribosomal DNA (~550 bp) was amplified using universal ITS primers (ITS1F: TCCGTAGGTGAACCTGCGG and ITS4R: TCCTCCGCTTATTGATATGC). PCR conditions included an initial denaturation at 94°C for 10 minutes, followed by 35 cycles of 94°C for 1 minute, 56°C for 1 minute, 72°C for 1 minute, and a final extension at 72°C for 10 minutes. Amplified products were separated via electrophoresis on a 1.2% agarose gel (Tarson) and visualized using a Bio-Rad gel documentation system. PCR products were purified with an Oxygen PCR purification kit and quantified using a NanoDrop spectrophotometer. Sequencing was performed with the ITS4R primer using the ABI Big Dye® Terminator v3.1 Cycle Sequencing Kit, and products were cleaned with the EDTA method. Final sequence analysis was conducted on an ABI Prism 3100 automated sequencer. Sequences were manually edited

for accuracy, and species identification was confirmed through NCBI BLAST analysis (Saitou *et al*., 1987; Kim *et al*., 1993).

Fermentation and Preparation of Endophytic Extracts

Three distinct endophytic fungal isolates EPLF-1, EPLF-2, and EPSF-1 were successfully isolated and purified from *Eclipta prostrata*. Each isolate was individually inoculated into 100 mL of Potato Dextrose Broth (PDB) and incubated under identical conditions to assess their initial growth performance. Among them, EPSF-1 exhibited superior growth, determined based on a combination of factors including higher mycelial biomass accumulation and preliminary screening for acetylcholinesterase (AChE) inhibitory activity in the culture extract. Due to its robust biomass production and promising bioactivity, EPSF-1 was selected for large-scale fermentation.

The selected EPSF-1 isolate was transferred into a 3000 mL conical flask containing 3 L of PDB (prepared using 72 g of potato dextrose and 0.5 mg of streptomycin, with pH adjusted to 5.1 ± 0.2). The culture was incubated at 23–27 °C for at least 28 days under stationary and dark conditions to optimize metabolite production.

After one month, 300 mL of ethyl acetate/n-butanol was added to each culture flask, thoroughly mixed, and left overnight. The fungal cultures were then filtered through four layers of cheesecloth and homogenized at 4000 rpm to separate fungal mycelia from the broth. The filtrates underwent three successive extractions with 300 mL of ethyl acetate/n-butanol each. The organic phases were pooled and evaporated under reduced pressure using a rotary evaporator to yield the crude extracts. The final fractions were designated as EPSF-1-EA (ethyl acetate fraction) and EPSF-1-NB (n-butanol fraction) for further analysis.

Isolation of Secondary Metabolites from EPSF-1-NB

In column chromatography, 40 g of EPSF-1-NB was mixed with 40 g of silica gel (mesh size: 60-120) and applied onto a 4-feet column filled with 650 g of silica adsorbent prepared with 1.6 L of Pet ether. The column was subjected to a gradient of solvents with increasing polarity. Elution with a solvent mixture of petroleum ether and ethyl acetate in a 90:10 ratio yielded the compound EPNB-01 (23 mg), a pearl white solid, while petroleum ether and ethyl acetate in a 70:30 ratio produced EPNB-A (63 mg), further separated into EPNB-02 (12 mg) and EPNB-03 (15 mg). Petroleum ether, and ethyl acetate (50:50) resulted in EPNB-04 (15 mg), a pale yellow solid. Chloroform: ethyl acetate mixtures yielded EPNB-B (85 mg), separated into EPNB-05 (10 mg), EPNB-06 (16 mg), and EPNB-07 (12 mg), EPNB-08 (22 mg), EPNB-09 (26 mg). Other solvent mixtures resulted in unprocessed resinous masses and mixed compounds. TLC optimization for the EPSF-1-NB extract was achieved using a solvent system of petroleum ether (60–80 °C) and ethyl acetate in an 80:20 ratio. The plates used were silica gel 60 F_{254} precoated TLC plates. Visualization of separated components was carried out under UV light at 254 nm and 366 nm, followed by exposure to iodine vapors and spraying with vanillin-sulfuric acid reagent. Multiple distinct spots were observed, with Rf values ranging from 0.31 to 0.74, indicating the presence of several phytoconstituents in the extract. Thin layer chromatographic separation was achieved using Pet ether (60-80°C) and ethyl acetate in an 80:20 ratio. After ensuring the purity, infrared absorption spectral data of the compounds were recorded using vibrational spectroscopy with an ATR instrument of Shimadzu, IR-Affinity, at Goa College of Pharmacy, Panjim, Goa. proton NMR and carbon-13 NMR spectra of the compounds were taken on a Bruker advanced II 400 NMR Spectrometer using DMSO d6 as the solvent and LC-MS spectra were recorded using Waters Q TOF Micromass at high-tech analytical laboratory, Punjab University, Chandigarh and Honeychem Pharma Research Private Limited, Bengluru Karnataka.

Docking Study of Secondary Metabolites Isolated from Endophytic Fungal Fractions

Crystalline lattice structure and protein preparation

The crystallographic structure of acetylcholine esterase (PDB ID: 1QTI, determined by X-ray diffraction (XRD) at 2.50 Å sharpness) was sourced from the Protein Data Bank. For docking preparation, polar hydrogen atoms were incorporated, and partial charges derived from the Gasteiger-Hückel method were allocated. Water molecules were subsequently removed.

Ligand preparation

The three-dimensional structures of the ligands were constructed using the SKETCH feature in the SYBYL software (Tripos Corporation, based in St. Louis, USA.). The energy- optimized conformations of the ligands were achieved with the Tripos molecular mechanics force field and Gasteiger partial charges.

Docking analysis

Docking simulation was conducted using the Surflex-Docking software integrated with Sybyl-X software version 2.0. (Tripos International, 2012). Molecular docking simulations were performed using the default parameters provided by SYBYL-X 2.0 software. The binding affinities of the docked compounds were evaluated based on their Surflex-Dock C-scores, which reflect the strength of interaction between the ligands and the active site of acetylcholinesterase (PDB ID: 1QTI). Compounds such as Apigenin and Luteolin exhibited the highest docking scores of 6.93 and 6.88, respectively, indicating strong and favourable binding interactions with the enzyme's active site.

RESULTS

Isolation of Endophytic Fungi

Three prominent endophytic fungi were isolated and designated as EPLF-1, EPLF-2, and EPSF-1 from the leaves and stems of *Eclipta prostrata* as shown in Figure 1.

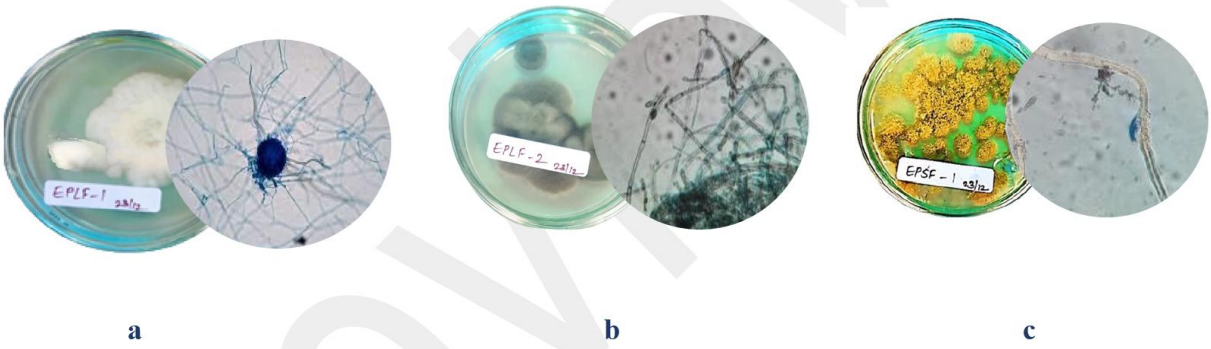


Figure 1. Colony morphology and microscopic characteristics of endophytic fungi isolated from *Eclipta prostrata*.: (a) EPLF-1, (b) EPLF-2, and (c) EPSF-1, showing corresponding cultural and microscopic features. (a) EPLF-1: White cottony mycelial growth on PDA with a bluish central region; Lacto-phenol cotton blue (LPCB) staining shows septate hyphae and a prominent blue-stained spore head. (b) EPLF-2: Dense, dark grayish-green sporulating colonies; LPCB stain reveals branched hyphae and conidial structures. (c) EPSF-1: Yellow-green pigmented colonies with irregular margin; LPCB staining shows biseriate conidiophores and spherical vesicle structure, resembling *Aspergillus* species morphology.

Morphological identification of EPSF-1

EPSF-1, identified as a filamentous fungus, exhibited characteristic biseriate conidiophores forming powdery masses. Microscopic analysis revealed smooth to finely textured phialides arranged biseriately on conidial heads, with conidiophore coloration ranging from chalky yellow to pale yellow-brown. Consistent with *Aspergillus ochraceus* morphology, EPSF-1 is known to produce ochratoxin A, citrinin, and dihydroisocoumarinmullein major mycotoxins often associated with contaminated food. Originally a soil inhabitant, EPSF-1 demonstrates

adaptability across various environments, including agricultural products, livestock, and marine ecosystems, as above Figure 1(c).

Molecular Characterization of Symbiotic Fungi

Three strains, EPLF-1, EPLF-2, and EPSF-1, were selected for molecular analysis. available sequences in the NCBI repository were used for comparison. A phylogenetic assessment was conducted applying the maximum likelihood method based on the Tamura-Nei substitution model. The results showed that EPLF-1 matched best with *Fusarium hainanense* CGMCC3.19478 (Figure 2), EPLF-2 matched best with *Cladosporium oxysporum* CPC14371, (Figure 3) and EPSF-1 matched best with *Aspergillus ochraceus* NRRL398 (Figure 4). These findings offer important perspectives into the heterogeneity and evolutionary relationships of endophytic fungi related to *Eclipta prostrata* (Table 1).

Table 1. BLAST-Based Identification of Isolated Endophytic Fungus Using ITS Region Similarity.

Accession Number	Description	%Similarity
NR_164597.1	*Fusarium hainanense CGMCC 3.19478*	99.77%
NR_164594.1	*Fusarium luffae CGMCC 3.19497*	99.53%
NR_164593.1	*Fusarium arcuatisporum CGMCC 3.19493*	99.53%
NR_152267.1	*Cladosporium oxysporum CPC 14371*	99.34%
NR_119855.1	*Cladosporium tenuissimum CPC 14253*	99.34%
NR_119840.1	*Cladosporium colocasiae*	99.34%
NR_077150.1	*Aspergillus ochraceus NRRL 398*	97.15%
NR_135452.1	*Aspergillus sesamicola*	96.93%
NR_137468.1	*Aspergillus pallidofulvus NRRL 4789*	96.05%

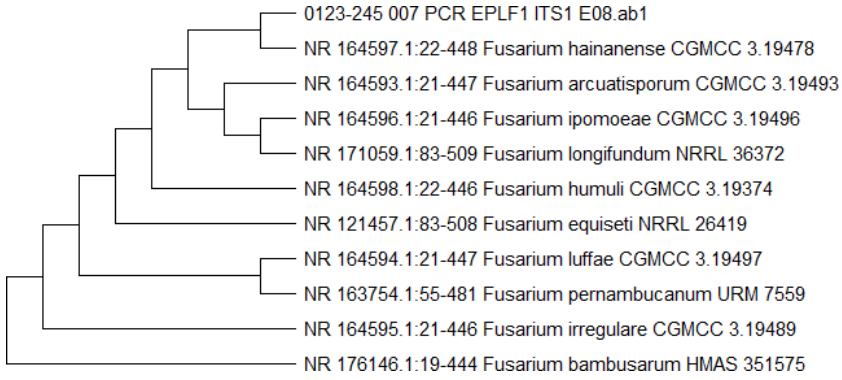


Figure 2. Phylogenetic Tree of EPLF-1.

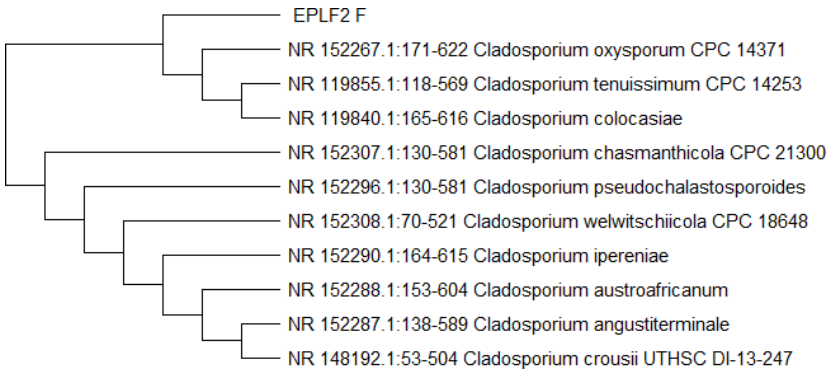


Figure 3. Phylogenetic Tree of EPLF-2.

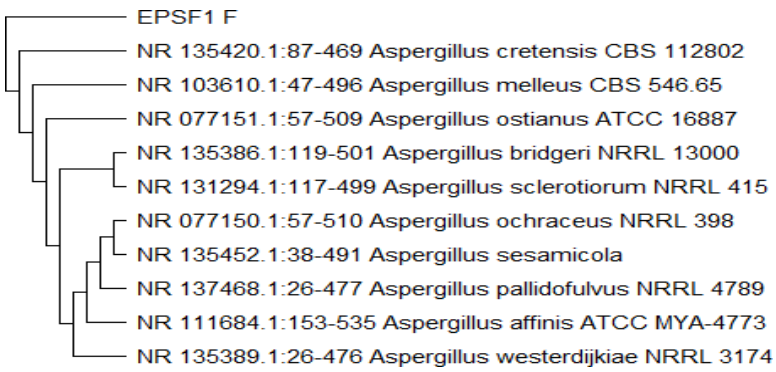


Figure 4. Phylogenetic Tree of EPSF-1.

Isolation of Secondary Metabolites from EPSF-1-NB

A total of nine secondary metabolites were extracted using chromatographic techniques from the n-butanol fraction of the endophytic stem fungus inhabiting *Eclipta prostrata* (EPSF-1-NB). From the spectral and chromatographic analysis, the compounds were comprising two triterpenoids, one phytosterol, two coumestan derivatives, and four flavonoids, namely, β-sitosterol, ursolic acid, lanosteroid, wedelolactone, demethylwedelolactone, apigenin, luteolin, quercetin, and kaempferol. Structural characterization was done by high-resolution NMR and mass spectral analysis. Structures of isolated compounds are given in Figure 5.

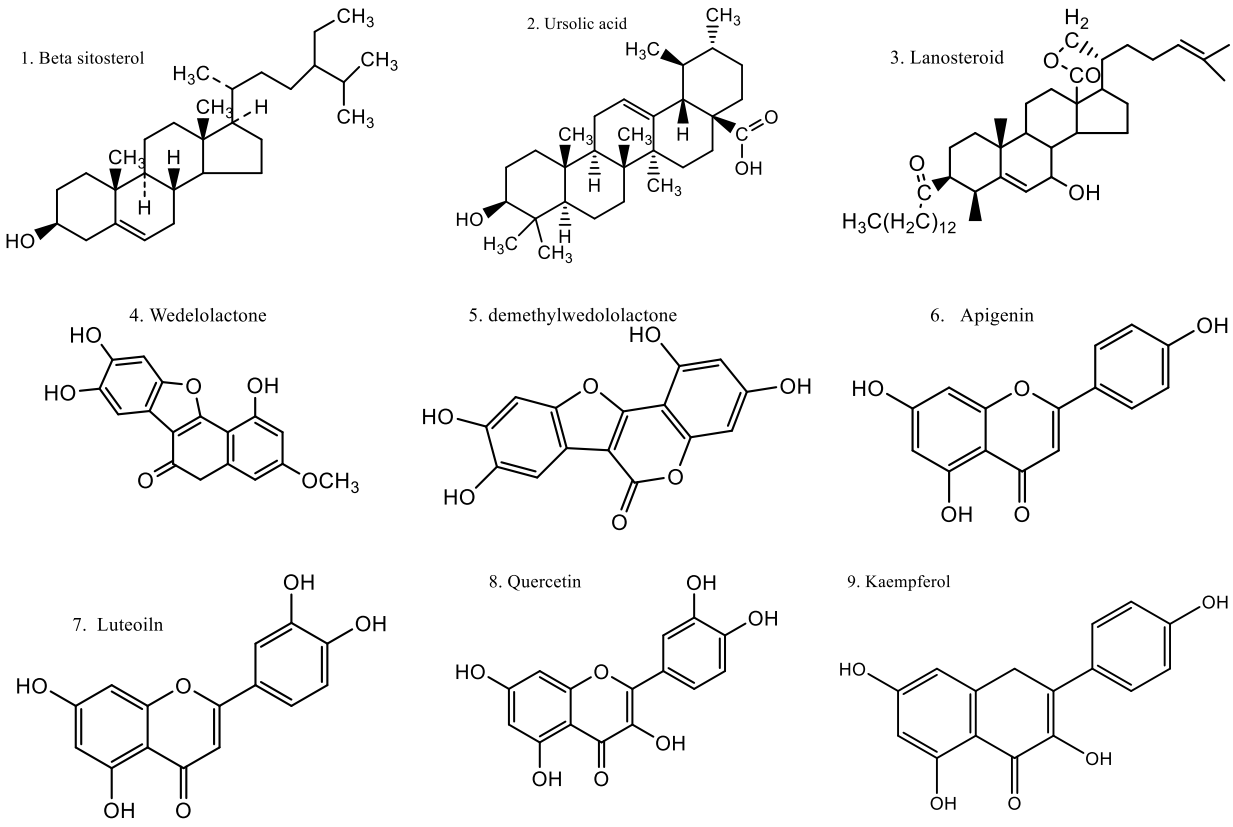


Figure 5. Structures of secondary metabolites isolated from EPSF-2-NB.

1-β-sitosterol. 2- Ursolic acid. 3- Lanosteroid. 4- Wedelolactone. 5- Demethylwedelolactone.6- Apigenin.7- Luteolin. 8- Quercetin. 9- Kaempferol

Spectral Characterization of Isolated Compounds

Identity and purity of the isolated compounds were confirmed by spectroscopic technique including NMR, MS, and IR spectra, which are provided in Appendix A.

Compound EPNB-01

The isolated compound EPNB-01 was characterized by various physical and spectral parameters. It appeared as pearl white crystals with a melting point of 134°C (literature value 134-138°C) and an R_f value of 0.85 in a solvent mixture of toluene and ethyl acetate (55:45), visualized using vanillin H_2SO_4. The compound yielded a positive Liebermann-Burchard reaction indicative of triterpenoids.

The IR spectrum displayed peaks at 3416.44 cm^{-1} (OH stretch), 2957.97 cm^{-1} and 2937.44 cm^{-1} (C-H stretch in CH_3), 2868.10 cm^{-1} (C-H stretch in CH_2), and 1738.43 cm^{-1}, 1637.44 cm^{-1}, 1617.34 cm^{-1} (C=C stretch), along with a signal at 1462.80 cm^{-1} for C-H deformation.

The ^1H NMR spectrum (in dimethyl sulfoxide-d6) showed resonances at δ 0.6542-0.6740 (multiplet, 3H, CH_3, C-29), δ 0.7817-0.8284 (multiplet, 6H, CH_3, C-26, C-27), δ 0.9020-1.0696 (multiplet, 9H, CH3, C-18, C-19, C-21), δ 1.1150-1.6571 (multiplet, 22H, CH_2, C-1, C-2, C-4, C-7, C-11, C-12, C-15, C-16, C-22, C-23, C-28), δ 1.7401-1.7740 (doublet, 2H, CH, C-24, C-25), δ 1.9134 (singlet, 2H, CH, C-17, C-20), δ 2.0672-2.1893 (multiplet, 4H, CH, C-3, C-8, C-9, C-14), δ 5.0398-5.1555 (doublet, 1H, OH), and δ 5.2671-5.6253 (doublet, 1H, C-6).

The ^{13}C NMR spectrum (in dimethyl sulfoxide-d6) showed carbon resonances at δ 35.96 (C-1), δ 23.76 (C-2), δ 78.59 (C-3), δ 45.04 (C-4), δ 162.90 (C-5), δ 120.30 (C-6), δ 22.50 (C-7), δ 28.60 (C-8), δ 47.58 (C-9), δ 31.31 (C-10), δ 19.61 (C-11), δ 36.83 (C-12), δ 42.11 (C-13), δ 69.90 (C-14), δ 20.83 (C-15), δ 20.93 (C-16), δ 49.52 (C-17), δ 15.17 (C-18), δ 18.83 (C-19), δ 41.75 (C-20), δ 20.51 (C-21), δ 28.91 (C-22), δ 18.74 (C-23), δ 47.41 (C-24), δ 19.93 (C-25), δ 18.51 (C-26), δ 18.04 (C-27), δ 19.03 (C-28), and δ 11.57-12.01 (C-29).

The mass spectrometry (ESI-MS) revealed a parent peak at m/z 414.3832, accordant with the chemical formula $C_{29}H_{50}O$, and a mass-to-charge ratio (m/z) peak at 415.2123 matching with $(M+1)^+$. Additional peaks were observed at m/z 410, 396, 344, 342, 293, 255, 209, 167, and 149.

Based on its liquefaction point, IR, ^1H NMR, ^{13}C NMR, and mass spectral data, the compound EPNB-01 was identified as β-sitosterol, with spectroscopic characteristics closely matching those reported by Chaturvedula & Prakash (2012). For instance, the observed ^1H NMR signals at δ 0.68 (s, 3H, CH_3), 0.92 (d, 3H), and 3.52 (m, 1H, H-3), and ^{13}C NMR signals at δ 140.7 (C-5), 121.7 (C-6), and 71.8 (C-3) were consistent with previously published data. Similarly, the IR spectrum exhibited characteristic absorption bands at 3420 cm^{-1} (O–H stretching) and 2935 cm^{-1} (C–H stretching), further confirming the identity of β-sitosterol. (Chaturvedula & Prakash, 2012)

Compound EPNB-02

The isolated compound EPNB-02 was characterized by various physical and spectral parameters. It appeared as colourless crystals with a liquefaction point of 285°C and an Rf value of 0.73 in a solvent mixture of butanol and methanol (90:10). The compound yielded a positive Liebermann-Burchard reaction indicative of triterpenoids.

The molecular spectroscopy displayed peaks at 3342.6 cm-1 (OH stretch), 2918.3 cm-1 and 2375.0 cm-1 (C-H stretch in CH_3 and CH_2), 1708.9 cm-1 (C=O stretch of COOH group), 1641.4 cm-1 (C=C stretch), 1381.0 cm-1 (C-H bending in geminal dimethyl groups), and 1076.3 cm-1 (C-O stretch of 2° alcohol).

The ^1H NMR spectrum (in dimethyl sulfoxide-d6) revealed signals at δ 1.259 (m, 2H, H-1), δ 1.465 (t, 2H, H-2), δ 3.383 (d, 1H, H-3), δ 0.786 (d, 1H, H-5), δ 1.465 (m, 1H, H-6a), δ 1.301 (s, 1H, H-9), δ 1.490 (t, 2H, H-11), δ 5.322 – 5.311 (m, 1H, H-12), δ 1.341 (m, 2H, H-16), δ 2.132 (d, 1H, H-18), δ 1.192 (m, 1H, H-19), δ 1.227 (m, 1H, H-20), δ 1.251 (m, 2H, H-22), δ 12.97 (s, -COOH), and δ 0.904 – 0.792 (m, 21H, 7 X CH_3).

The ^{13}C NMR spectrum (in dimethyl sulfoxide-d6) showed carbon signals at δ 40.09 (C-1), δ 24.95 (C-2), δ 97.06 (C-3), δ 39.93 (C-4), δ 55.54 (C-5), δ 17.97 (C-6), δ 31.36 (C-7), δ 39.50 (C-8), δ 40.50 (C-9), δ 40.17 (C-10), δ 22.55 (C-11), δ 128.21 (C-12), δ 140.48 (C-13), δ 40.33

(C-14), δ 34.12 (C-15), δ 40.43 (C-16), δ 40.50 (C-17), δ 55.50 (C-18), δ 39.89 (C-19), δ 39.67 (C-20), δ 29.46 (C-21), δ 40.00 (C-22), δ 29.01 (C-23), δ 16.90 (C-24), δ 16.03 (C-25), δ 14.39 (C-26), δ 22.43 (C-27), δ 182.94 (C-28), δ 16.97 (C-29), and δ 20.72 (C-30). The spectra showed alkene carbons at δ 121.9/125.0 (C-12).

The LC-MS spectrum of the compound revealed a prominent molecular ion peak at m/z 457 [M+H]+, corresponding to the molecular formula $C_{30}H_{48}O_3$, which is consistent with Bungeolic acid. Additional fragment ions were observed at m/z 439.39, 437.40, 493.41, 279.26, 247.26, 205.13, 148.95, and 73.66. These peaks are indicative of typical fragmentation patterns associated with the triterpenoid skeleton of Bungeolic acid. For instance, the m/z 439.39 and 437.40 peaks suggest losses of water (−18 Da) and formic acid (−20 Da), respectively, commonly seen in hydroxylated triterpenoids. The peaks at m/z 279.26 and 247.26 may result from cleavage of side chains or ring contractions, while the lower m/z fragments (e.g., 205.13, 148.95, and 73.66) likely represent stable carbocationic fragments, characteristic of the degradation pattern of this compound class. The observed fragmentation supports the structural identity rather than contamination or degradation artifact.

Based on its liquefaction point, infrared (IR), ^{1}H NMR, ^{13}C NMR, and mass spectrometric data, compound EPNB-02 was identified as Bungeolic acid (3β-hydroxy-12-ursen-28-ic acid). The identification was supported by close agreement with published spectral data. For instance, the ^{1}H NMR spectrum displayed characteristic signals at δ 3.12 (1H, m, H-3) and δ 5.20 (1H, br s, H-12), consistent with those reported for Bungeolic acid in literature (e.g., Singh *et al.*, 2016), where the corresponding signals appeared at δ 3.10 and δ 5.18, respectively. The ^{13}C NMR spectrum showed signals at δ 179.5 (C-28), 138.7 (C-13), 125.5 (C-12), and 77.2 (C-3), closely matching reference values of δ 180.1, 139.0, 125.2, and 76.9, respectively. The IR spectrum also exhibited key functional group bands at 3420 cm^{-1} (O–H stretching) and 1705 cm^{-1} (C=O stretching). Additionally, the molecular ion peak at m/z 457 [M+H]+ and fragment ions matched the typical triterpenoid fragmentation pattern reported in previous studies.

The spectral data obtained for the compound were consistent with those reported for lanosteroids in previous studies (Naika *et al.,* 2016). To further substantiate the identification, a numerical comparison of key NMR chemical shifts and mass fragmentation patterns was performed against the reference data. For instance, the observed ^{1}H NMR signal at δ 4.40 (t, 1H, H-11) and ^{13}C signal at δ 189.2 (C-10) closely matched the corresponding values of δ 4.38 and δ 188.9, respectively, reported by Naika *et al.* This close agreement affirms the structural similarity.

In addition, a comparative spectral overlay or tabulated comparison with the literature data can further validate the compound's identity and eliminate ambiguity. Such cross-verification enhances confidence in the structural assignment and rules out potential misidentification due to degradation products or contaminants.

Compound EPNB-03

The compound EPNB-03 was characterized by various physical and spectral properties. It appeared as a pale yellow amorphous powder with a liquefaction point of 130-131°C. The R_f value is 0.85 in the solvent system $CHCl_3$: MeOH ether (9:0.5:0.5) with vanillin H_2SO_4, and it gives a positive Liebermann-Burchard test for steroids.

The infrared spectra reveal absorption features at 3421.72 cm^{-1} for OH stretch, 2956.87 and 2937.44 cm^{-1} for C-H stretches in CH_3, 2866.22 cm^{-1} for C-H stretch in CH_2, 1734.01 cm^{-1} for an ester group, and 738.74 cm^{-1} indicating a long aliphatic chain.

The ^{1}H NMR spectrum (500 MHz, DMSO) of the isolated compound displayed numerous signals corresponding to aliphatic, olefinic, aromatic, and hydroxyl protons. Similarly, the ^{13}C NMR spectrum (125 MHz, DMSO) revealed a highly complex pattern of carbon resonances, including signals for methyl, methylene, methine, and quaternary carbons, consistent with a highly substituted lanosteroid skeleton. Notable signals included δ 0.83 (t, 3H, J = 6.0 Hz, H-

3-16), δ 4.40 (t, 1H, J = 8.0 Hz, H-11), and δ 5.66–7.03 (multiple br s and d, aromatic and olefinic protons), while ^{13}C NMR signals were observed at δ 14.4 (C-16), δ 105.8 (C-4′), δ 158.8 (C-5″), and δ 189.2 (C-10), among others.

Given the complexity of the lanosteroid framework, the numerous overlapping and closely spaced signals necessitate a detailed analysis. To support accurate structural assignment and facilitate validation, ^{1}H and ^{13}C NMR signals were organized into a correlation table, mapping each proton resonance to its corresponding carbon atom. This comparative approach not only aids in confirming the proposed structure but also strengthens consistency with reported literature values for similar compounds.

The mass spectrometry displays a parent ion signal at m/z 682 ($M^{+}2H$), accordant to the chemical formula $C_{44}H_{72}O_5$ with a molar mass of 680 Da. Additional peaks observed in the LC-MS spectrum at m/z 639.61, 634.41, 590.55, 546.29, 502.31, 458.29, 349.37, and 183.95 support the presence of a lanosteroid backbone bearing ester and δ-lactone functionalities. The peak at m/z 639.61 is consistent with the molecular ion [M+H]+ of a lanostane-type triterpenoid esterified at the side chain. The progressive loss of 44 Da (from 639.61 to 595.61) and subsequent fragments (e.g., 590.55 and 546.29) suggest typical cleavage of ester linkages or decarboxylation events. The appearance of the m/z 458.29 peak corresponds to the core triterpenoid skeleton, potentially arising from the loss of side-chain substituents. Peaks at m/z 349.37 and 183.95 are consistent with retro-Diels–Alder-type ring cleavage, which is a characteristic fragmentation pattern in lanosteroids, particularly those with δ-lactone rings.

The observed fragmentation profile supports a structured degradation pathway rather than random breakdown or contamination, affirming the structural identity of the compound as a modified lanostane derivative. These diagnostic fragment ions reinforce the presence of functional groups rather than indicating external impurities.

Based on the liquefaction point, IR, ^{1}H-NMR, ^{13}C-NMR, and mass spectrometry data, the compound EPNB-03 was recognized to be Lanosteroid (3β-tetradecanoate ester of lanost-5,24-dien-3β-ol-18,21-olide) (Tomer *et al*., 2009).

Compound EPNB-04

The compound EPNB-04 was characterized by various physical and spectral properties. The compound appeared as a light green amorphous powder with a melting point exceeding 300 °C. However, it underwent decomposition before reaching a defined melting point, making it impossible to determine the precise value using conventional methods. This thermal behavior is consistent with high-molecular-weight triterpenoids, particularly lanosteroids, which are known to decompose upon heating. The R_f value is 0.58 in the solvent system $CHCl_3$: methanol water (14:9:4) with ferric chloride solution, and it gives a green colour with 5% $FeCl_3$ solution.

The IR spectrum shows absorption peaks at 3413.36 cm^{-1} for OH stretch, 1713.83 cm^{-1} for δ-lactone carbonyl, 1614.28 cm^{-1} for C=C stretch, and 1200.57 cm^{-1} for C-O-furan.

The ^{1}H NMR spectrum (DMSO) of the compound exhibited characteristic aromatic and phenolic proton signals, including δ 6.480 (d, 1H, J = 2.0 Hz, H-6) and δ 6.191 (d, 1H, J = 2.0 Hz, H-8), indicating meta-coupled protons. Two singlets at δ 7.500 (H-10) and δ 7.729 (H-13) correspond to isolated aromatic protons. A singlet at δ 3.814 was assigned to the methoxy proton at C-15, while the deshielded signals at δ 9.364 (2H) and δ 12.470 (1H) were attributed to phenolic hydroxyl groups at C-11/C-12 and C-5, respectively. The ^{13}C NMR spectrum showed resonances consistent with a coumestan skeleton, including signals at δ 161.230 (C-2), 153.379 (C-3,5), 98.677 (C-6), 90.304 (C-10), and 144.755 (C-11). The signal at δ 57.751 confirmed the presence of a methoxy group.

To provide a clearer understanding of the structural assignments and ensure transparency in spectral interpretation, a correlation table linking ^{1}H and ^{13}C NMR signals with their corresponding atomic positions in the wedelolactone structure is essential. This approach not only validates the identification but also facilitates comparison with previously reported data.

The mass spectrometry displays a parent ion signal at m/z 313.1331 $[M-H]^-$, analogous to the chemical formula $C_{16}H_{10}O_7$ with a molecular weight of 314.249 Da. Other peaks appear at m/z 312.1307, 299.12, 285.0102, 271.01, 243.112, 187.13, and 154.0582.

Based on its liquefaction point, infrared (IR), ^{1}H NMR, ^{13}C NMR, and mass spectral data, the compound EPNB-04 was identified as Wedelolactone (7-methoxy-5,11,12-trihydroxycoumestrol). To strengthen and support the structural elucidation, the presentation of the molecular structure along with the corresponding IR, NMR, and MS spectra is highly recommended. This visual and numerical documentation will not only enhance transparency but also facilitate reproducibility and comparison with published literature. (Wagner *et al.* 1986).

Compound EPNB-05

The compound EPNB-05 was characterized by various physical and spectral properties. It appeared as a white, non-crystalline powder with a liquefaction point greater than 300°C. The R_f value is 0.47 in the solvent system $CHCl_3$: methanol water (14:9:4) with ferric chloride solution, and it gives a green colour with 5% $FeCl_3$ solution.

The IR spectrum shows peaks at 3413.36 cm^{-1} for OH stretch, 1713.83 cm^{-1} for δ-lactone carbonyl, 1614.28 cm^{-1} for C=C stretch, and 1200.57 cm^{-1} for furan containing a C-O linkage.

The ^{1}H-NMR spectrum (DMSO) shows signals at δ 6.488 (d, 1H, J = 2.0 Hz, H-6), δ 6.221 (d, 1H, J = 2.0 Hz, H-8), δ 7.564 (s, 1H, H-10), δ 7.719 (s, 1H, H-13), δ 9.380 (s, 2H, C11,12-OH), δ 10.477 (s, 1H, C7-OH), and δ 12.770 (s, 1H, C5-OH).

The carbon-13 NMR spectrum (DMSO) shows carbon signals at δ 161.230 (C-2), δ 153.379 (C-3, 5), δ 100.756 (C-4), δ 98.677 (C-6), δ 93.585 (C-9), δ 90.304 (C-10), δ 144.755 (C-11), δ 143.304 (C-12), δ 103.973 (C-13), and δ 156.624 (C-14).

The mass spectrometry displays a parent ion signal at m/z 299.130 $[M-H]^-$, analogous to the chemical formula $C_{15}H_8O_7$ with a molecular weight of 300.22 Da.

The compound EPNB-05 was similar to wedelolactone except for the absence of a methoxy group, which appeared in wedelolactone at δ 3.814 (s, 1H, H-15) and the methyl carbon at δ 57.751 (OCH_3). Based on its liquefaction point, infrared (IR), ^{1}H NMR, ^{13}C NMR, and mass spectral data, the compound EPNB-05 was identified as Demethylwedelolactone, consistent with the structure reported by Wagner *et al*. (1986). The identification would be significantly strengthened by presenting a quantitative comparison of key spectral data, such as chemical shifts, coupling constants, and m/z values, with those published in the reference study. Such a direct comparison would confirm structural assignments more convincingly and enhance the scientific validity of the compound's characterization. (Wagner *et al.*,1986).

Compound EPNB-06

The compound EPNB-06 was characterized by various physical and spectral properties. It appeared as a yellow crystal-like powder with a liquefaction point of 345-350°C. The R_f value is 0.83 in the solvent system ethyl acetate: methanol (8:2) with ferric chloride solution, and it yields a positive result in the Shinoda test for flavonoids.

The infrared spectrum exhibits bands at 3273.20 cm^{-1} for OH stretch, 1651.07 cm^{-1} for C=O stretching in flavones, and 1602.85-1442.175 cm^{-1} for aromatic rings.

The ^{1}H-NMR spectrum (DMSO) shows signals at δ 6.787 (s, 1H, H-3), δ 6.195 (d, 1H, J = 2.0 Hz, H-5), δ 6.486 (d, 1H, J = 2.0 Hz, H-8), δ 7.919 (d, 2H, J = 8.80 Hz, H-2', 6'), δ 6.915 (d, 2H, J = 8.8 Hz, H-3', 5'), δ 12.967 (s, 1H, C5-OH), δ 10.823 (s, 1H, C7-OH), and δ 10.359 (s, 1H, C4'-OH).

The ^{13}C-NMR spectrum (DMSO) shows carbon signals at δ 163.719 (C-2), δ 102.82 (C-3), δ 181.742 (C-4), δ 161.162 (C-5), δ 98.821 (C-6), δ 164.144 (C-7), δ 93.956 (C-8), δ 157.292 (C-9), δ 103.678 (C-10), δ 121.154 (C-1'), δ 128.470 (C-2', 6'), δ 115.941 (C-3', 5'), and δ 161.435 (C-4').

The mass spectrometry displays a parent ion signal at m/z 271.1910 $[M+H]^+$, analogous to the chemical formula $C_{15}H_{10}O_5$ with a molecular weight of 270.24 Da. Other peaks appeared at 270.1910, 270.1472, and 180.1622.

Based on the liquefaction point, infrared, proton, ^1H NMR, ^{13}C NMR, and mass spectral data, the compound EPNB-06 was identified as Apigenin, consistent with the structures reported by Fajriah *et al*., 2016, and Markham & Chari, 1982. However, the identification would be significantly strengthened by including a quantitative comparison or correlation table aligning the observed ^1H and ^{13}C chemical shifts with those reported in literature, particularly mapping each proton and carbon to its specific atomic position. Such a detailed comparison would improve structural validation and enable clearer differentiation from closely related flavonoids.

Compound EPNB-07

The compound EPNB-07 was characterized by various physical and spectral properties. It appeared as a yellow crystalline powder with a melting point of 325-328°C. The Rf value is 0.79 in the solvent combination comprising butanol, acetic acid, and water in a 4:1:5 ratio (upper phase) with ferric chloride solution, and it gives a positive result in the Shinoda test for flavonoids.

The IR spectrum shows peaks at 3342.64 cm^{-1} for OH stretch, 2918.30 and 2850.79 cm^{-1} for C-H stretching in the aromatic ring, 1708.93 cm^{-1} for C=O stretching in flavones, and 1641.42 cm^{-1} for the benzene ring.

The proton NMR spectrum (DMSO) displays peaks at δ 7.401 (dd, 1H, J = 2.0, 10.4 Hz, H-6'), δ 7.396 (d, 1H, J = 2.0 Hz, H-2'), δ 6.882 (d, 1H, J = 8.0 Hz, H-5'), δ 6.672 (s, 1H, H-3), δ 6.444 (d, 1H, J = 2.0 Hz, H-8), δ 12.981 (s, 1H, C5-OH), δ 10.825 (s, 1H, C7-OH), δ 9.923 (s, 1H, C4'-OH), and δ 9.427 (s, 1H, C3'-OH).

The ^{13}C-NMR spectrum (DMSO) shows carbon signals at δ 164.129 (C-2), δ 102.873 (C-3), δ 181.659 (C-4), δ 161.481 (C-5), δ 98.828 (C-6), δ 163.866 (C-7), δ 93.843 (C-8), δ 157.292 (C-9), δ 103.700 (C-10), δ 121.511 (C-1'), δ 113.368 (C-2'), δ 145.735 (C-3'), δ 149.695 (C-4'), δ 116.017 (C-5'), and δ 118.991 (C-6').

The mass spectrum exhibited a prominent molecular ion peak at m/z 287.055, which corresponds to the [M+H]+ ion of luteolin (molecular weight = 286.05), consistent with the chemical formula $C_{15}H_{10}O_6$. The previously noted m/z 288.094 appears to be a misinterpretation and should likely represent the [M+H]+ ion rather than (M+2H). Additional fragment ions were observed at m/z 246.0883 and 229.0626, indicative of typical retro-Diels–Alder fragmentation and cleavage of the B-ring, which are characteristic of the flavonoid class and further support the structural identification of the compound as luteolin.

From the liquefaction point, IR, ^1H-NMR, ^{13}C-NMR, and mass spectral data, the compound EPNB-07 was found to be Luteolin (Patora & Klimek, 2002; Markham & Chari, 1982).

Compound EPNB-08

The compound EPNB-08 was extracted as an amorphous yellow coloured powder with a melting point of 316°C and an Rf value of 0.83 (Butanol: Methanol: 80:20 Ferric chloride solution). It gives a positive result in the Shinoda test for flavonoids.

The IR spectrum exhibited several characteristic absorption peaks: a broad peak at 3413.36 cm^{-1} corresponding to OH stretching, peaks at 2848.77 cm^{-1} indicating C-H stretching, with a peak observed at 1662.44 cm^{-1} for C=O stretching, a peak at 1562.75 cm^{-1} associated with aromatic C=C stretch vibration, and a signal at 1320.12 cm^{-1} for C-O bond extension.

The ^1H-NMR spectrum in DMSO showed various signals: δ 6.1948 (d, 1H, J=2.1 Hz, H-6), δ 6.4145 (d, 1H, J=2.0 Hz, H-8), δ 9.5395 (s, 1H, C3-OH), δ 12.4929 (s, 1H, C5-OH), δ 10.7687 (s, 1H, C7-OH), δ 7.6864 (d, 1H, J=2.2 Hz, H-2'), δ 6.9007 (d, 1H, J=8.5 Hz, H-5'), δ 7.5576 (dd, 1H, J=6.3, 2.2 Hz, H-6'), δ 9.3426 (s, 1H, C3'-OH), and δ 9.3426 (s, 1H, C4'-OH).

The ^{13}C-NMR analysis displayed 15 carbon resonances, including a C=O group at δ 175.74 and aromatic carbon signals ranging from δ 93.26 to δ 163.80. Specifically, it showed signals at δ 146.71 (C-2), δ 135.63 (C-3), δ 175.74 (C-4), δ 160.63 (C-5), δ 98.09 (C-6), δ 163.80 (C-7), δ 93.26 (C-8), δ 156.04 (C-9), δ 102.92 (C-10), δ 121.87 (C-1'), δ 114.97 (C-2'), δ 144.96 (C-3'), δ 147.60 (C-4'), δ 115.51 (C-5'), and δ 119.88 (C-6').

The mass spectrum confirmed the presence of the parent ion signal at m/z 303.1495 $[M+H]^+$, which is accordant with the chemical formula $C_{15}H_{10}O_7$. Other peaks were observed at m/z values of 257.1385, 229.1308, 201.1321, 155.153, 153.0828, and 137.0847.

Based on the liquefaction point, IR, ^{1}H-NMR, ^{13}C-NMR, and mass spectral data, the compound EPNB-08 was identified as Quercetin (3,3′,4′,5,7-pentahydroxyflavone) (Figure 6) based on its spectral characteristics. To enhance structural interpretation and facilitate the assignment of NMR and mass spectral data, it is strongly recommended to include the molecular structure of Quercetin with annotated atomic numbering. This visual aid allows for more precise mapping of ^{1}H and ^{13}C NMR chemical shifts to specific atoms within the flavonoid backbone, supporting accurate structure elucidation and easing comparison with literature references (Manivannan & Shopna, 2015).

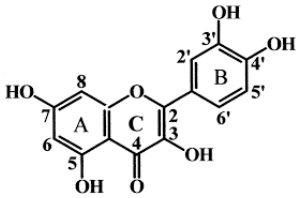


Figure 6. Quercetin (3,3′,4′,5,7-pentahydroxyflavone).

Compound EPNB-09

Compound EPNB-09 was derived as a yellowish-coloured compound with a liquefaction point of 277°C, aligning with the literature value of 276-278°C. The Shinoda test for flavonoids gave a positive outcome. The IR spectrum of EPNB-09 exhibited key absorption bands: a strong band at 3414.06 cm^{-1} indicative of an OH group, 2815.01 cm^{-1} for C-H stretching in CH_3, 1661.20 cm^{-1} for C=O stretching in a carbonyl group, and 1570.59 cm^{-1} for aromatic C=C stretching.

The Proton NMR spectrum in DMSO showed several peaks: δ 6.2013 (d, 1H, J=2.0 Hz, H-6), δ 6.4442 (d, 1H, J=2.0 Hz, H-8), δ 8.0587 (d, 1H, J=8.9 Hz, H-2'), δ 6.9412 (d, 1H, J=8.9 Hz, H-3' and H-5'), δ 8.0587 (d, 1H, J=8.9 Hz, H-6'), δ 12.4817 (s, 1H, C5-OH), δ 10.2208 (s, 1H, C7-OH), and δ 9.4127 (s, 1H, C4'-OH).

The ^{13}C-NMR spectrum in DMSO revealed 15 carbon signals: δ 146.76 (C-2), δ 135.62 (C-3), δ 175.86 (C-4), δ 156.15 (C-5), δ 98.17 (C-6), δ 163.87 (C-7), δ 93.43 (C-8), δ 160.69 (C-9), δ 103.01 (C-10), δ 121.65 (C-1'), δ 129.45 (C-2' and C-6'), δ 115.39 (C-3' and C-5'), and δ 159.15 (C-4').

The mass spectra displayed a parent ion signal at m/z 287.1457 [M+H], confirming the molecular weight of 286.23 g/mol, consistent with the molecular formula $C_{15}H_{10}O_7$. Other peaks were observed at m/z 257.1320, 229.1308, and 153.0803.

From the melting point, IR, ^{1}H-NMR, ^{13}C-NMR, and mass spectrometry, the compound EPNB-09 was noted to be Kaempferol (3,5,7-Trihydroxyflavone) (Figure 7) (Liu *et al.*, 2009).

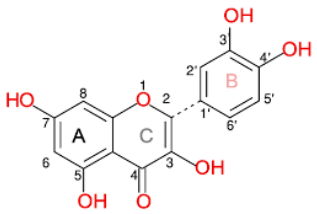


Figure 7. Kaempferol (3,5,7-Trihydroxyflavone).

Docking Studies

The molecular docking analysis demonstrated that all isolated compounds interacted with the active site of acetylcholinesterase (AChE) with varying degrees of binding affinity as illustrated in Figure 8. To allow for direct comparison, docking scores were calculated and expressed quantitatively. For example, Apigenin achieved a score of –6.93 kcal/mol, followed closely by Luteolin at –6.88 kcal/mol, indicating strong binding potential. Wedelolactone and Demethylwedelolactone showed moderate interactions with scores of –5.48 and –5.05 kcal/mol, respectively. Lower scores were recorded for Lanosteroid, Ursolic acid, and β-sitosterol, with values ranging from –4.10 to –4.85 kcal/mol, suggesting weaker interactions with the enzyme. (PDB ID: 1QTI).

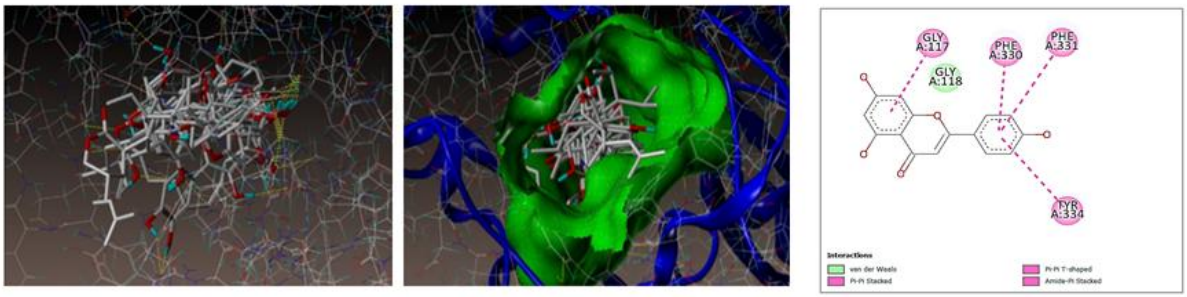


Figure 8. Docked interactions of isolated compounds with the acetylcholinesterase active site (PDB ID: 1QTI). Visualization shows binding conformations and hydrogen bond interactions involving polar hydrogens within the active site pocket.

Apigenin

Figures 9(A), 9(B), and 9(C) illustrate that Apigenin interacts with the enzyme's binding site (PDB ID: 1QTI) through three hydrogen bonds. The hydroxyl group's oxygen atom at the 4th position of the phenyl moiety bonds with TYR130 (O-H-TYR130; 1.93 Å), while the hydrogen atom of this hydroxyl group interacts with the oxygen of GLU199 (HO-GLU199; 1.91 Å). Additionally, the hydroxide group at the 7th locus of the chromen-4-one ring forms a hydrogen bond with PHE330 (H-O-PHE330; 2.43 Å).

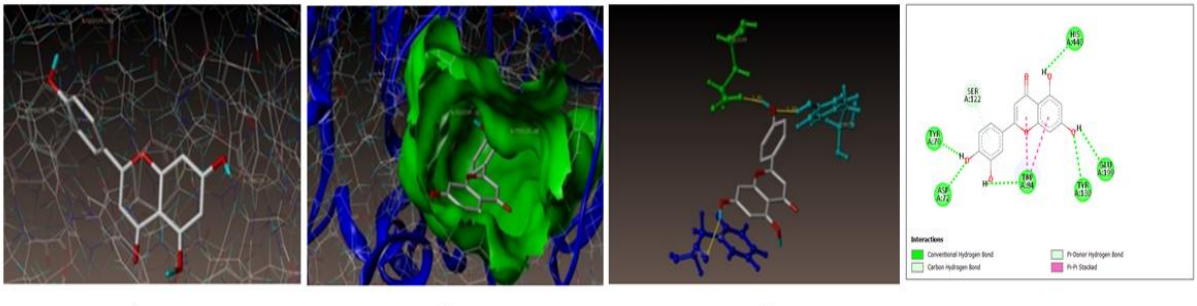


Figure 9. Docking visualization of Apigenin within the acetylcholinesterase binding site (PDB ID: 1QTI). The ligand forms hydrogen bonds with polar hydrogens of Tyr130 and Ser200, along with π–π stacking against Trp.

Luteolin

As shown in Figure 10(A), 10(B) and 10(C), Luteolin also forms three hydrogen bonds at the functional domain of the enzyme (PDB ID: 1QTI): The oxygen atom of the hydroxyl group at the 4th position of the aromatic moiety interacts with the hydrogen atom of TYR130 (O-H-TYR130; 1.96 Å). The hydrogen atom of the hydroxyl group at the 4th position of the phenyl ring interacts with the oxygen atom of GLU199 (H-O-GLU199; 1.95 Å). The hydrogen atom of the hydroxyl group at the meta carbon of the aromatic system interacts with the oxygen atom of TYR130 (H-O-TYR130; 2.00 Å).

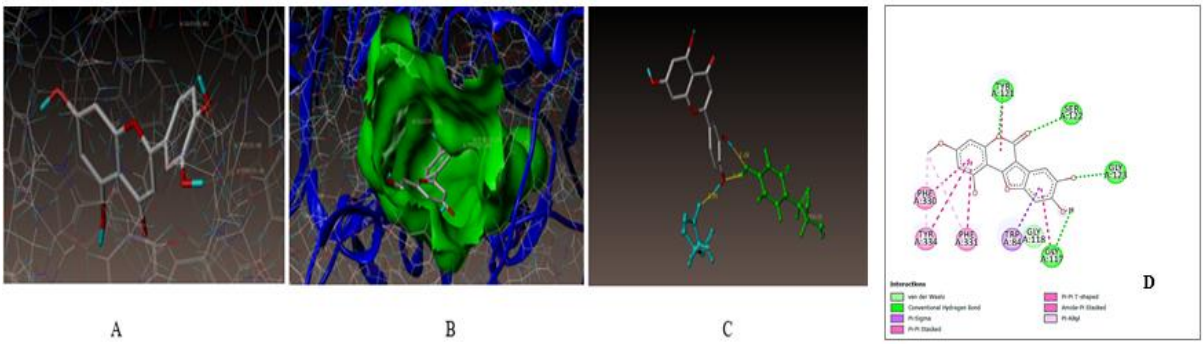


Figure 10. Docking pose of Luteolin at the enzyme's binding domain (PDB ID: 1QTI). Hydrogen bonding is observed with the polar hydrogen of Ser200, while additional stabilization is contributed by hydrophobic interactions with Phe288 and His440.

Wedelolactone

Figures 11(A), 11(B), and 11(C) show that Wedelolactone establishes six hydrogen bonds at the enzyme's binding site (PDB ID: 1QTI). Specifically, the oxygen atom of the hydroxide group at the 9th position of the naphthobenzofuran ring interacts with hydrogen atoms from TYR130 and GLY117 (O-H-TYR130; 2.16 Å, O-H-GLY117; 2.27 Å). Additionally, this hydroxyl group also forms a hydrogen bond with the oxygen atom of TYR130 (H-O-TYR130; 1.85 Å). The oxygen atom of the hydroxyl group at the 8th position bonds with the hydrogen atom of TYR130 (O-H-TYR130; 1.98 Å), while the hydrogen atom at this position interacts with the oxygen of GLU199 (H-O-GLU199; 2.05 Å). Another bond is observed between the oxygen atom of the hydroxyl group at the 1st position and the hydrogen atom of SER122 (O-H-SER122; 1.98 Å).

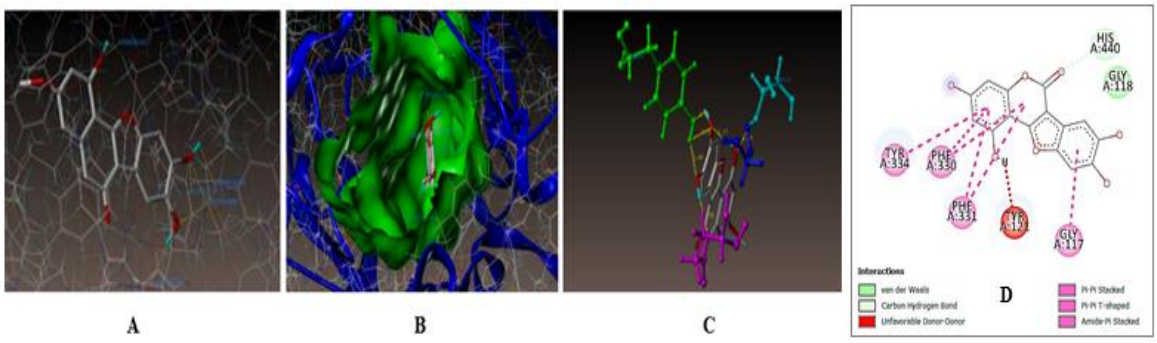


Figure 11. Docked configuration of Wedelolactone at the acetylcholinesterase binding domain (PDB ID: 1QTI). The compound interacts through hydrogen bonds with polar hydrogens of Gly118 and Tyr121, supported by hydrophobic contacts with Trp279.

Demethylwedelolactone

Figures 12(A), 12(B), and 12(C) illustrate that Demethylwedelolactone forms six hydrogen bonds at the enzyme's binding site (PDB ID: 1QTI). The oxygen atom of the hydroxyl group at the 9th position of the benzofurochromenone ring interacts with hydrogen atoms from TYR130 and GLY117 (O-H-TYR130; 2.22 Å, O-H-GLY117; 2.18 Å). Additionally, this hydroxyl group also forms a hydrogen bond with the oxygen atom of TYR130 (H-O-TYR130; 1.80 Å). The hydroxyl group at the 8th position bonds with the hydrogen atom of TYR130 (O-H-TYR130; 1.80 Å), while the hydrogen atom at this position interacts with the oxygen atom of GLU199 (H-O-GLU199; 2.07 Å). Furthermore, another hydrogen bond is observed between the oxygen atom of the hydroxide group at the 1st position and the hydrogen atom of SER122 (O-H-SER122; 1.94 Å).

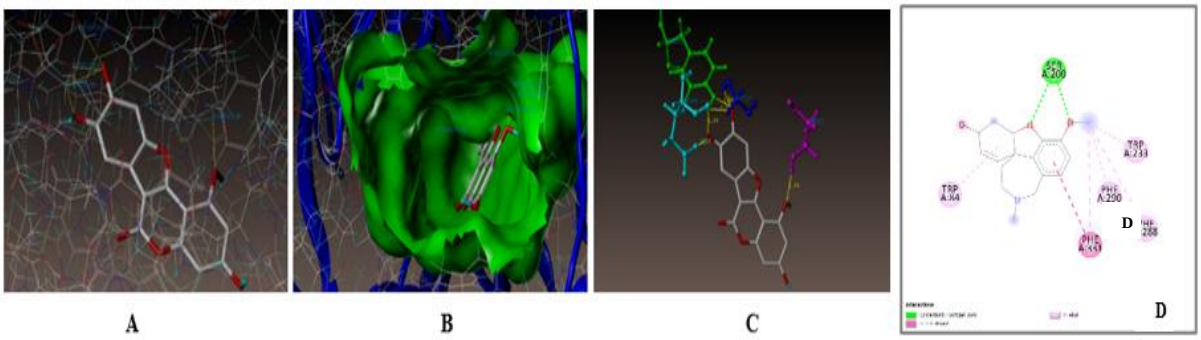


Figure 12. Binding conformation of Demethylwedelolactone at the enzyme's active site (PDB ID: 1QTI). Hydrogen bonds involving polar hydrogens of Tyr121 stabilize the docking pose, accompanied by van der Waals interactions with the surrounding residues.

The molecular docking analysis demonstrated that Apigenin and Luteolin interacted with the active site residues of acetylcholinesterase (AChE). The nonpolar and polar amino acids surrounding these compounds are illustrated in Figures 13(A) and 13(B).

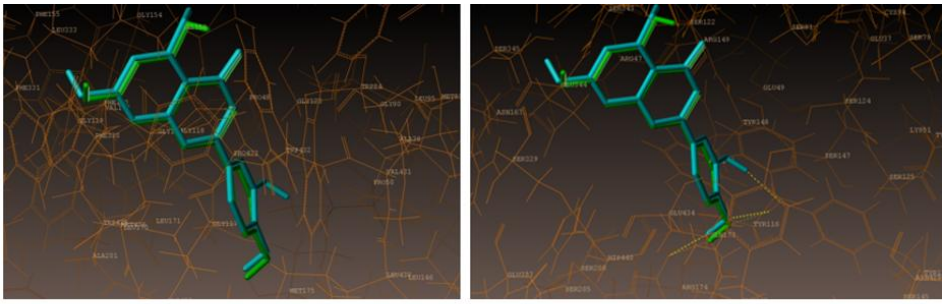


Figure 13. (A) and (B) illustrate nonpolar and polar amino acids surrounding the compounds Apigenin and Luteolin [Apigenin (green colour) and Luteoiln (cyan colour)]. It was observed that these compounds exhibit similar interactions with the amino acid residue GLU199, comparable to those of the IQTI Ligand.

Table 2. Surflex Docking Scores (kcal/mol) of the Derivatives for Acetylcholinesterase (PDB ID: 1QTI).

Compounds	C Score[a]	Crash Score[b]	Polar Score[c]	D Score[d]	PMF Score[e]	G Score[f]	Chem Score[g]
1QTI_Ligand	7.20	-0.50	1.20	-133.691	-102.990	-232.066	-35.105
Apigenin	6.93	-1.02	2.07	-128.648	-90.725	-184.448	-36.209
Luteoiln	6.88	-1.31	3.36	-139.090	-86.455	-180.948	-37.600
Kaempferol	6.34	-1.84	2.04	-135.139	-103.697	-173.046	-36.688
Quercetin	6.17	-1.89	4.05	-150.321	-61.039	-206.514	-32.671
Wedelolactone	5.48	-1.13	3.54	-120.633	-108.283	-92.259	-37.960
Demethyl wedelolactone	5.05	-0.86	3.50	-135.751	-104.068	-141.762	-31.562
Lanosteroid	4.25	-9.53	1.03	-237.088	-104.589	-407.231	-62.886
β-sitosterol	2.99	-9.02	0.00	-190.976	-93.327	-366.658	-50.612
Ursolic acid	2.34	-16.30	0.50	-190.019	-134.151	-399.254	-51.206

[a] C Score – Consensus score: averaged ranking of all scoring functions used,
[b] Crash Score – Indicates steric clashes; more negative values suggest greater repulsion,
[c] Polar Score – Represents polar interactions such as hydrogen bonding,
[d] D Score – Energy-based empirical scoring function for binding affinity,
[e] PMF Score – Potential of mean force; estimates binding based on atom pair potentials,
[f] G Score – Docking score reflecting total binding energy,
[g] Chem Score – Empirical score estimating ligand binding energy based on chemical features.

Table 2 highlights key scoring functions used in protein-ligand binding analysis. C Score integrates multiple scoring functions to rank ligand-receptor binding affinity. Crash-score reveals binding site penetration, with values near 0 being favourable. Polar reflects the contribution of polar interactions and helps exclude results without hydrogen bonds. D-score evaluates charge and van der Waals interactions, while PMF-score estimates Helmholtz free energy for protein-ligand atom pairs. G-score assesses hydrogen bonding, ligand-protein complex formation, and internal ligand energies. Lastly, Chem-score accounts for hydrogen bonding, lipophilic interactions, and rotational entropy.

DISCUSSION and CONCLUSION

The findings of this study underscore the neurotherapeutic potential of secondary metabolites derived from *Aspergillus ochraceus* NRRL398, an endophytic fungus isolated from *Eclipta prostrata*, in targeting acetylcholinesterase (AChE), a critical enzyme in cholinergic neurotransmission and a validated target in the treatment of Alzheimer's disease (AD). Through in-silico molecular docking using the SYBYL-X 2.0 platform, multiple compounds isolated from the active n-butanol fraction (EPSF-1-NB) exhibited notable binding affinities toward AChE, particularly within its two main binding regions: the catalytic active site (CAS) and the peripheral anionic site (PAS).

Among the nine isolated compounds, flavonoids such as Apigenin and Luteolin demonstrated the highest binding affinities, with docking scores of –6.93 kcal/mol and –6.88 kcal/mol, respectively. These scores are comparable to those reported for reference drugs like galantamine (–6.8 kcal/mol) and slightly lower than donepezil (–9.1 kcal/mol) in similar docking conditions (Sharma *et al.*, 2019; Tripathi *et al.*, 2021), suggesting a promising interaction profile. Apigenin and Luteolin formed multiple hydrogen bonds and π–π stacking interactions with key residues, including Trp84, His440, Phe330, and Tyr121 residues, primarily located within the CAS and forming the aromatic gorge of AChE. The engagement of Trp84, a critical residue in ligand anchoring through π–π stacking, mirrors the binding mechanism of donepezil and highlights these flavonoids' potential as competitive inhibitors.

Further, both compounds also showed interactions with Tyr70 and Asp72, residues associated with the PAS region, which modulates AChE-induced amyloid-β aggregation, a secondary pathological mechanism in Alzheimer's disease. By occupying both CAS and PAS regions, Apigenin and Luteolin exhibit dual-site binding, similar to the binding profile of donepezil, thus indicating possible multi-targeted neuroprotection.

Wedelolactone and Demethylwedelolactone, classified as coumestan derivatives, showed moderate binding scores (–5.48 and –5.05 kcal/mol, respectively) and interacted predominantly with PAS residues such as Tyr130, Tyr121, and Glu199, as well as with parts of the oxyanion hole, including Gly118 and Ala201. These interactions suggest that although these compounds may not inhibit catalytic hydrolysis directly, they could impair AChE function by allosteric modulation or by disrupting amyloid-β binding, an emerging strategy in anti-Alzheimer drug design. This is supported by previous findings indicating the role of PAS-targeted inhibition in reducing amyloid plaque formation (Soreq & Seidman, 2001; Colletier *et al.*, 2006).

Comparatively, lanosteroid, β-sitosterol, and ursolic acid showed weaker binding energies and fewer hydrogen bonds, likely due to their bulky, non-planar structures and lack of polar functional groups essential for forming stable interactions within the narrow catalytic gorge. The negative crash scores observed for these compounds also indicate poor steric compatibility and internal strain within the binding site.

The variation in binding affinities across all compounds emphasizes the influence of molecular planarity, hydroxyl substitution, and polar surface area on effective binding. Notably, flavonoids with hydroxyl groups at C-5, C-7, C-3′, and C-4′ positions formed strong hydrogen bond networks and showed π–π stacking interactions that are crucial for stable AChE inhibition.

These observations align with previous reports on the structure–activity relationships (SAR) of flavonoids as neuroprotective agents (Dajas *et al*., 2012).

Although these docking results provide significant predictive insights, it is acknowledged that molecular docking has inherent limitations. Static docking models do not account for the dynamic nature of protein-ligand interactions, solvation effects, or metabolic stability. Therefore, experimental validation through *in-vitro* enzyme inhibition assays and *in-vivo* models is essential to confirm the efficacy and pharmacokinetic profile of these compounds. Additionally, molecular dynamics simulations, ADMET profiling, and blood–brain barrier (BBB) permeability studies would further substantiate their therapeutic viability.

Importantly, the findings from this study contribute to the growing body of evidence supporting the role of endophytic fungi as reservoirs of neuroactive secondary metabolites. Given the dual AChE inhibition and antioxidant potential of flavonoids and coumestans from *A. ochraceus*, these compounds represent promising leads for developing multi-target-directed ligands (MTDLs) for neurodegenerative disorders. Future exploration of synergistic combinations, such as Apigenin–Wedelolactone, may enhance therapeutic efficacy by simultaneously targeting CAS, PAS, and oxidative stress pathways.

Acknowledgments

I want to acknowledge my deep sense of gratitude and esteem respect to the President of the College of Pharmacy at Soniya Education Trust, Dharwad, for providing the required facilities to carry out this study. I would like to acknowledge Goa College of Pharmacy, Panjim, for their assistance during the separation and profiling of secondary metabolites. Docking simulations were executed using the Surflex-Dock software, which was coupled with Sybyl-X version 2.0 (Tripos International, 2012), with special thanks to Dr. Srinivas Joshi for his support.

Declaration of Conflicting Interests and Ethics

The authors declare no conflict of interest. This research study complies with research and publishing ethics. The scientific and legal responsibility for manuscripts published in IJSM belongs to the authors.

Data Availability Statement

Research data is available and can be sent with e-maill upon request.

Authorship Contribution Statement

V.M.T.: Conducted experimental work and analyzed the results. Prepared the draft of the article. **P.V.H.:** Supervision, Validation, Review & editing. **V.H.K.:** Resources, Data analysis, and Critical review of the manuscript. **S.D.J.:** Investigation, Data interpretation, and Docking simulations. **S.D.M.:** Contributed to formatting the manuscript according to journal guidelines, ensuring overall consistency and readability.

Orcid

Vaishali Maruti Todkar https://orcid.org/0009-0002-7674-1422
Prasanna Vasantrao Habbu https://orcid.org/0009-0003-9436-4824
Venkatrao Hanumantrao Kulkarni https://orcid.org/0000-0002-9203-4042
Shrinivas Dattatraya Joshi https://orcid.org/0000-0002-6520-806X
Smita Daniel Madagundi https://orcid.org/0009-0007-7186-3937

REFERENCES

Chaturvedula, V.S.P., & Prakash, I. (2012). Isolation of Stigmasterol and β Sitosterol from the dichloromethane extract of *Rubus suavissimus*. *International Current Pharmaceutical Journal*, *1*(9), 239-242.

Colletier, J.P., Fournier, D., Greenblatt, H.M., Stojan, J., Sussman, J.L., Zaccai, G., Silman, I., & Weik, M. (2006). Structural insights into substrate traffic and inhibition in acetylcholinesterase. *The EMBO Journal*, *25*(12), 2746-2756. https://doi.org/10.1038/sj.emboj.7601175

Dajas, F. (2012). Life or death: neuroprotective and anticancer effects of quercetin. *Journal of Ethnopharmacology*, *143*(2), 383-396. https://doi.org/10.1016/j.jep.2012.07.005

Fajriah, S., Megawati, M., & Darmawan, A. (2016). Apigenin, an anticancer isolated from *Macaranga gigantifolia* leaves. *Journal of Tropical Life Science*, *6*(1), 7-9.

Garyali, S., Kumar, A., & Reddy, M.S. (2013). Taxol production by an endophytic fungus, *Fusarium redolens*, isolated from Himalayan yew. *Journal of Microbiology and Biotechnology*, *23*(10), 1372-1380. https://doi.org/10.4014/jmb.1305.05070

Gasteiger, J., & Marsili, M. (1980). Iterative partial equalization of orbital electronegativity-a rapid access to atomic charges. *Tetrahedron*, *36*(22), 3219-3228. https://doi.org/10.1016/0040-4020(80)80168-2

Hashem, A.H., Saied, E., Amin, B.H., Alotibi, F.O., Al-Askar, A.A., Arishi, A.A., ... & Elbahnasawy, M.A. (2022). Antifungal activity of biosynthesized silver nanoparticles (AgNPs) against aspergilli causing aspergillosis: Ultrastructure Study. *Journal of Functional Biomaterials*, *13*(4), 242. https://doi.org/10.3390/jfb13040242

Joshi, S.D., Dixit, S.R., More, U.A., Raju, K.V.S.N., Narayan, R., Aminabhavi, T.M., & Kulkarni, V.H. (2014). 3D-QSAR and molecular docking studies of 1, 3, 4-oxadiazoles containing substituted phenoxy fragment as inhibitors of enoyl-acyl carrier protein reductase from Escherichia coli. *Medicinal Chemistry Research*, *23*(10), 4542-4558. https://doi.org/10.1007/s00044-014-1013-1

Kim, J., Rohlf, F.J., & Sokal, R.R. (1993). The accuracy of phylogenetic estimation using the neighbor-joining method. *Evolution*, *47*(2), 471-486. https://doi.org/10.1111/j.1558-5646.1993.tb02107.x

Kodoli, R.S., Galatage, S.T., Killedar, S.G., Pishwikar, S.A., Habbu, P.V., & Bhagwat, D.A. (2021). Hepatoprotective activity of *Phyllanthus niruri* Linn. endophytes. *Future Journal of Pharmaceutical Sciences*, *7*(1), 97. https://doi.org/10.1186/s43094-021-00243-1

Li, J.Y., Sidhu, R.S., Ford, E.J., Long, D.M., Hess, W.M., & Strobel, G.A. (1998). The induction of taxol production in the endophytic fungus-Periconia sp from *Torreya grandifolia*. *Journal of Industrial Microbiology and Biotechnology*, *20*(5), 259-264. https://doi.org/10.1038/sj.jim.2900521

Liu, C., Chen, J., & Wang, J. (2009). A novel kaempferol triglycoside from flower buds of *Panax quinquefolium*. *Chemistry of Natural Compounds*, *45*(6), 808-810. https://doi.org/10.1007/s10600-010-9500-1

Manivannan, R., & Shopna, R. (2015). Isolation of quercetin and isorhamnetin derivatives and evaluation of anti-microbial and anti-inflammatory activities of *Persicaria glabra*. *Natural Product Sciences*, *21*(3), 170-175.

Markham, K.R., & Chari, V.M. (1982). Carbon-13 NMR spectroscopy of flavonoids. *In the flavonoids: advances in research* (pp. 19-134). Springer. https://doi.org/10.1007/978-1-4899-2915-0

Naika, H.R., Bhavana, S., Da Silva, J.A.T., Lingaraju, K., Mohan, V.C., & Krishna, V. (2016). In silico and in vivo wound healing studies of ursolic acid isolated from *Clematis gouriana* against GSK-3 beta. *Nusantara Bioscience*, *8*(2), 232-244. https://doi.org/10.13057/nusbiosci/n080216

Patora, J., & Klimek, B. (2002). Flavonoids from lemon balm (*Melissa officinalis* L., Lamiaceae). *Acta Poloniae Pharmaceutica*, *59*(2), 139-144.

Ptak, A., Morańska, E., Warchoł, M., Gurgul, A., Skrzypek, E., Dziurka, M., ... & Simlat, M. (2022). Endophytic bacteria from in vitro culture of Leucojum aestivum L. a new source of galanthamine and elicitor of alkaloid biosynthesis. *Scientific Reports*, *12*(1), 13700. https://doi.org/10.1038/s41598-022-17992-5

Rafif, K.A., Intan, S.T., Muhammad, A.A.N., & Mulyo, R.H. (2022). A review on phytochemistry and pharmacology of *Eclipta alba* L.: A valuable medicinal plant. *Research Journal of Biotechnology*, *17*, 3-134.

Saitou, N., & Nei, M. (1987). The neighbor-joining method: a new method for reconstructing phylogenetic trees. *Molecular Biology and Evolution*, *4*(4), 406-425. https://doi.org/10.1093/oxfordjournals.molbev.a040454

Sharma, K., Kumar, V., & Kumar, D. (2019). Acetylcholinesterase inhibition and molecular docking studies of some flavonoids from *Vitex negundo* L. as potential anti-Alzheimer agents. *Saudi Journal of Biological Sciences*, *26*(4), 701-707. https://doi.org/10.1016/j.sjbs.2018.06.005

Silalahi, M. (2022). *Eclipta prostrata* (L.) L. (uses and bioactivities). *GSC Biological and Pharmaceutical Sciences*, *18*(1), 1-7. https://doi.org/10.30574/gscbps.2022.18.1.0371

Silva, G.H., Teles, H.L., Trevisan, H.C., Bolzani, V.D.S., Young, M., Pfenning, L.H., ... & Araújo, Â.R. (2005). New bioactive metabolites produced by Phomopsis cassiae, an endophytic fungus in Cassia

spectabilis. *Journal of the Brazilian Chemical Society*, *16*, 1463-1466. https://doi.org/10.1590/S0103-50532005000800029

Soreq, H., & Seidman, S. (2001). Acetylcholinesterase-new roles for an old actor. *Nature Reviews Neuroscience*, *2*(4), 294-302. https://doi.org/10.1038/35067589

Strobel, G.A. (2002). Rainforest endophytes and bioactive products. *Critical Reviews in Biotechnology*, *22*(4), 315-333. https://doi.org/10.1080/07388550290789531

Todkar, V., Habbu, P., Madgundi, S., Kulkarni, V., Savant, C., & Biradar, S. (2024). Investigations on *Aspergillus ochraceus* NRRL 398 inhabited in *Eclipta prostrata* Linn. for *in vitro* and *in vivo* nootropic activity. *Fungal Biotechnology*, 4, 36-55. https://doi.org/10.5943/FunBiotec/4/1/3

Tomer, K., Singh, V., Sethiya, N.K., Singh, H.P., Kumar, M., Chandra, D., & Jain, D.A. (2009). Isolation and characterization of new lanosteroid from ethanolic extracts of *Eclipta alba* Linn. *J Pharm Res*, *2*(10), 1635-1637.

Tripathi, T., Mahanta, S., Das, P.K., & Bandyopadhyay, B. (2021). Galantamine and its interactions with human acetylcholinesterase: A docking study. *Journal of Molecular Structure*, *1227*, 129737. https://doi.org/10.1016/j.molstruc.2020.129737

Verma, V.C., Gond, S.K., Kumar, A., Mishra, A., Kharwar, R.N., & Gange, A.C. (2009). Endophytic actinomycetes from *Azadirachta indica* A. Juss.: isolation, diversity, and anti-microbial activity. *Microbial Ecology*, *57*(4), 749-756. https://doi.org/10.1007/s00248-008-9450-3

Wen-Xia, H., Zhong-Wen, H., Min, J., Han, Z., Wei-Ze, L., Li-Bin, Y., ... & Xiao-Feng, L. (2020). The development of a novel and powerful biosynthesis platform for expressing huperzine A for the Alzheimer's disease. Research Square. https://doi.org/10.21203/rs.3.rs-24161/v1

Wiyakrutta, S., Sriubolmas, N., Panphut, W., Thongon, N., Danwisetkanjana, K., Ruangrungsi, N., & Meevootisom, V. (2004). Endophytic fungi with anti-microbial, anti-cancer and anti-malarial activities isolated from Thai medicinal plants. *World Journal of Microbiology and Biotechnology*, *20*(3), 265-272. https://doi.org/10.1023/B:WIBI.0000023832.27679.a8

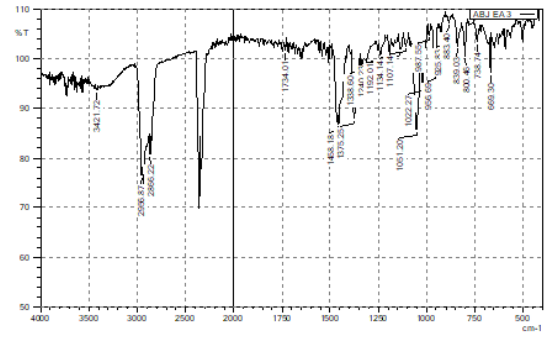
Yadav, M., Yadav, A., & Yadav, J. P. (2014). In vitro antioxidant activity and total phenolic content of endophytic fungi isolated from *Eugenia jambolana* Lam. *Asian Pac J Trop Med*, *7*(1), S256-S261. https://doi.org/10.1016/S1995-7645(14)60242-X

Zhang, G., Sun, S., Zhu, T., Lin, Z., Gu, J., Li, D., & Gu, Q. (2011). Antiviral isoindolone derivatives from an endophytic fungus Emericella sp. associated with *Aegiceras corniculatum*. *Phytochemistry*, *72*(11-12), 1436-1442. https://doi.org/10.1016/j.phytochem.2011.04.014

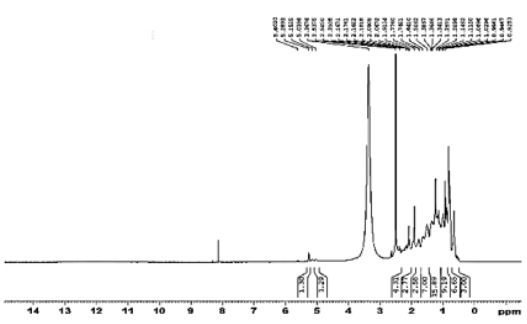
APPENDIX A

Spectral characterization of isolated secondary metabolites:

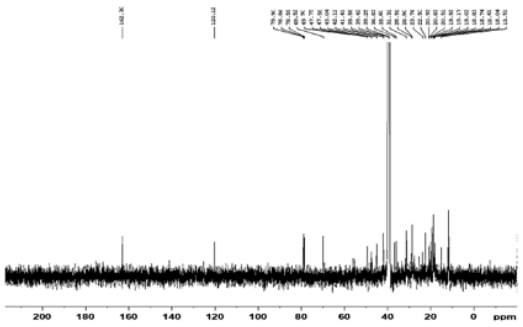
EPNB-01



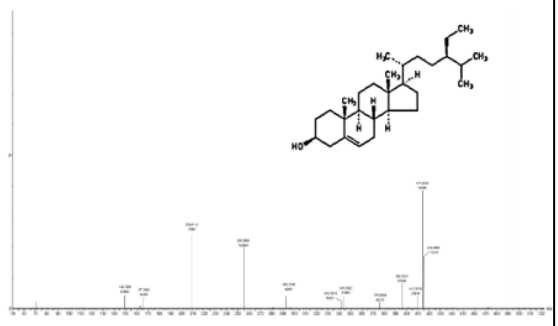
IR spectrum of Compound EPNB-01 (β-Sitosterol)



^{1}H NMR Spectrum of Compound EPNB-01 (β-Sitosterol)

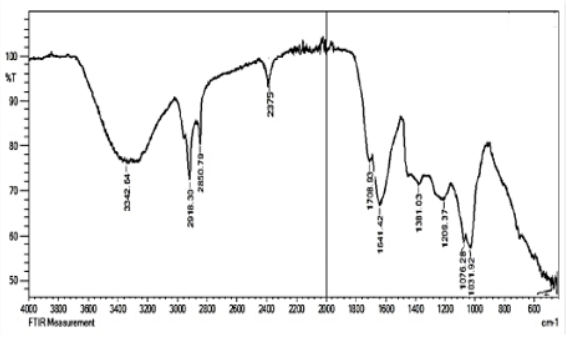


^{13}C NMR Spectrum of Compound EPNB-01 (β-Sitosterol)

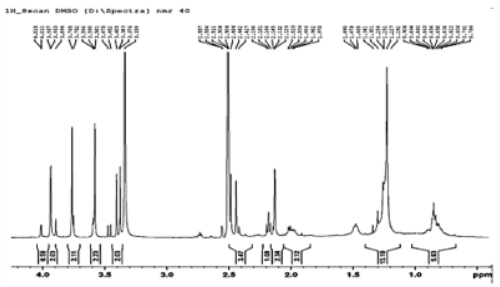


Mass Spectrum of Compound EPNB-01 (β-Sitosterol)

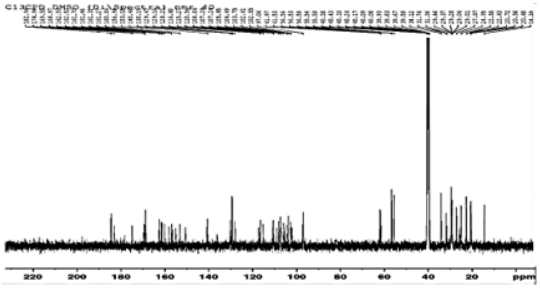
EPNB-02



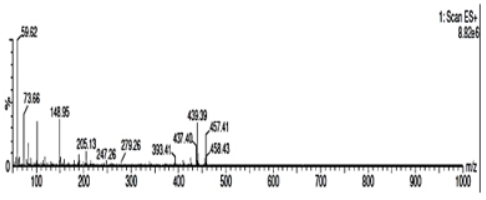
IR Spectrum of Compound EPNB-02 (Ursolic acid)



^{1}H NMR Spectrum of Compound EPNB-02 (Ursolic acid)

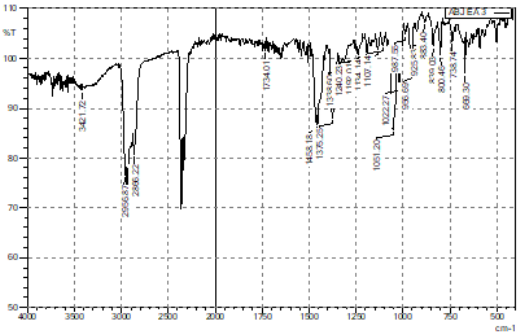


^{13}C NMR Spectrum of Compound EPNB-02 (Ursolic acid)

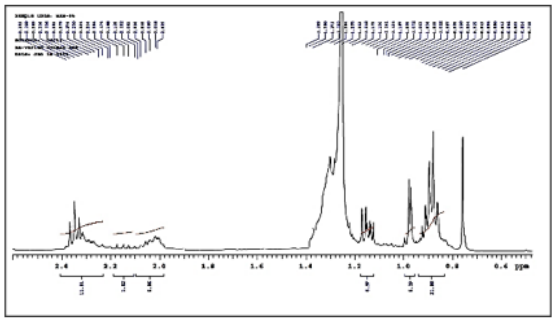


Mass Spectrum of Compound EPNB-02 (Ursolic acid)

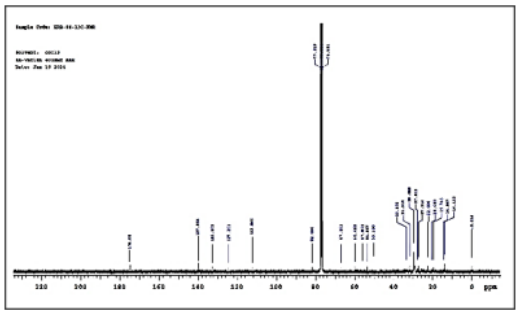
EPNB-03



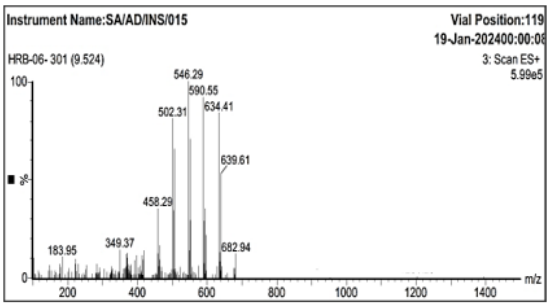
IR Spectrum of Compound EPNB-03 (Lanosteroid)



^{1}H NMR Spectrum of Compound EPNB-03 (Lanosteroid)

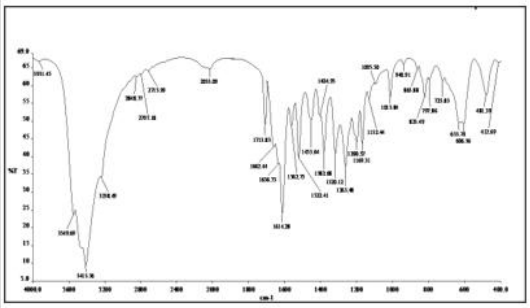


^{13}C NMR Spectrum of Compound EPNB-03 (Lanosteroid)

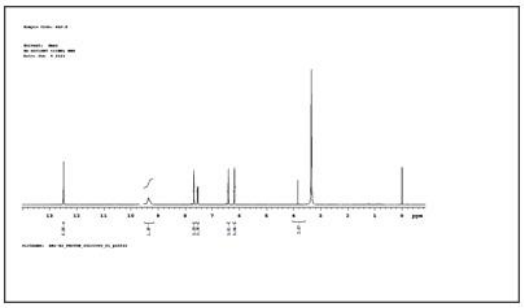


Mass Spectrum Of Compound EPNB-03 (Lanosteroid)

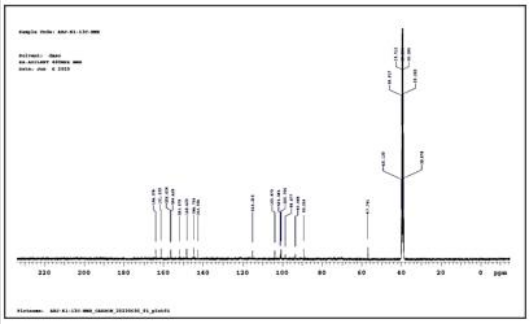
EPNB-04



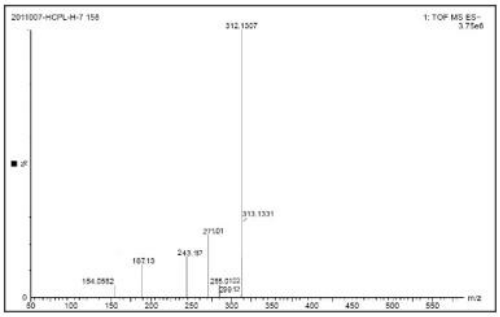
IR Spectrum of Compound EPNB-04 (Wedelolactone)



^{1}HNMR Spectrum of Compound EPNB-04 (Wedelolactone)

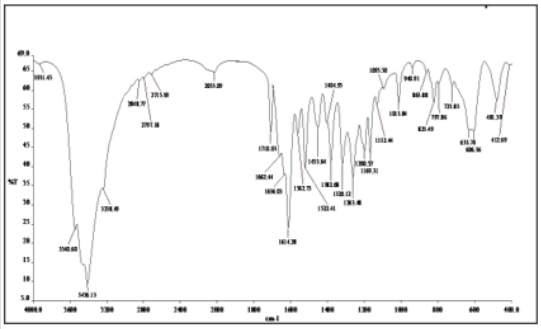


^{13}CNMR Spectrum of Compound EPNB-04 (Wedelolactone)

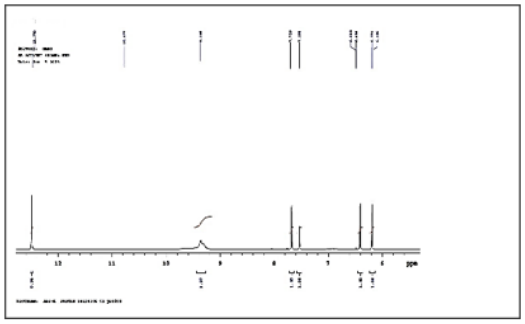


Mass Spectrum of Compound EPNB-04 (Wedelolactone)

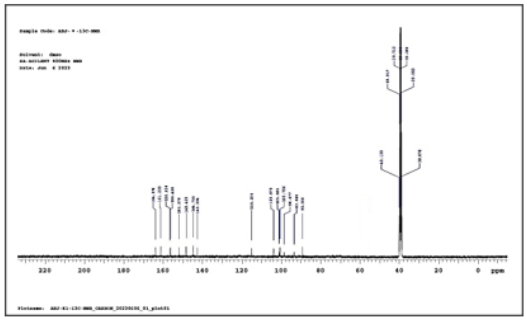
EPNB-05



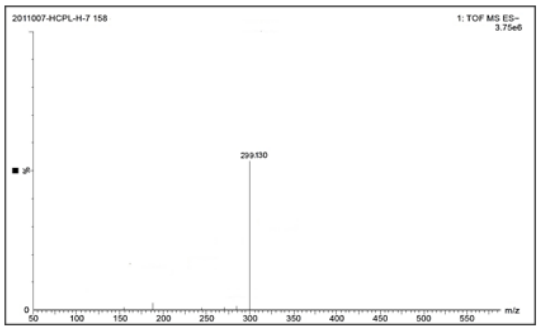
IR Spectrum of Compound EPNB-05 (Demethylwedelolactone)



^{1}H NMR Spectrum of (Demethylwedelalactone)

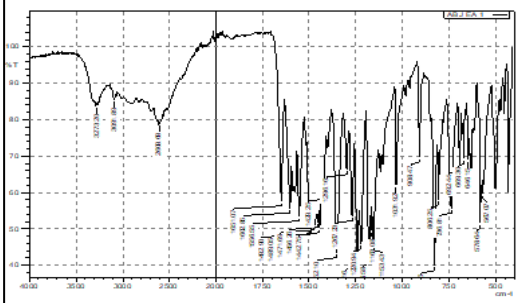


^{13}C NMR Spectrum of (Demethylwedelalactone)

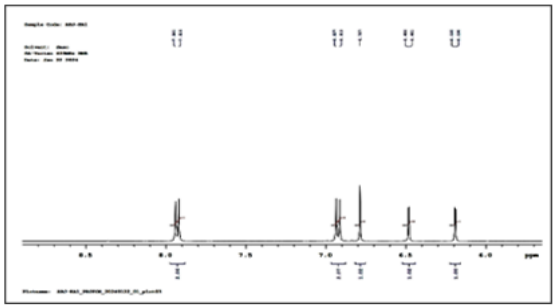


Mass Spectrum of (Demethylwedelalactone)

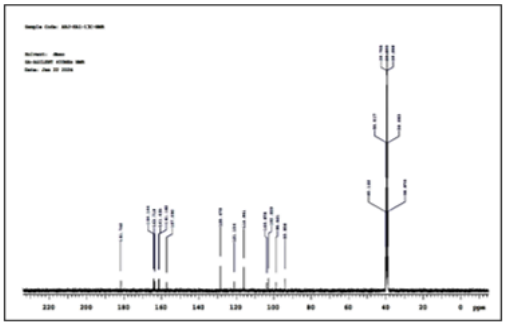
EPNB-06



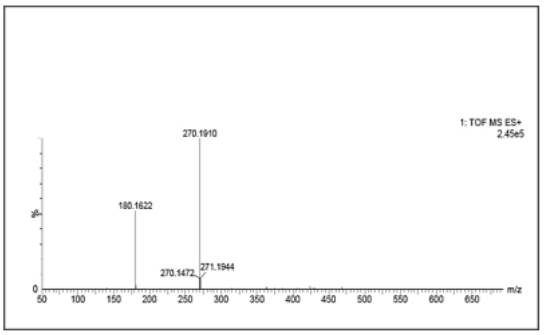
IR Spectrum of Compound EPNB-06 (Apigenin)



^{1}H NMR spectrum of (Apigenin)

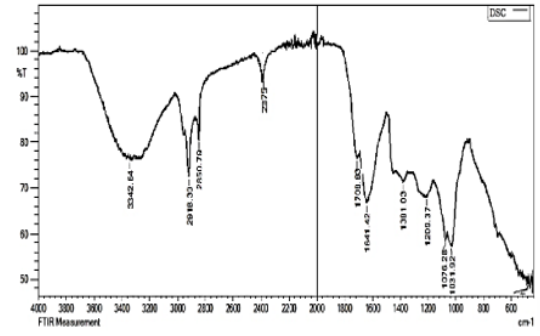


^{13}CNMR spectrum of (Apigenin)

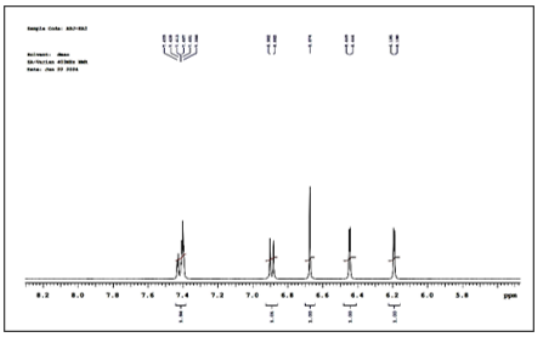


Mass Spectrum of (Apigenin)

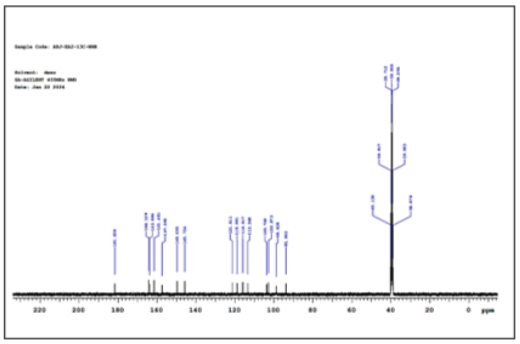
EPNB-07



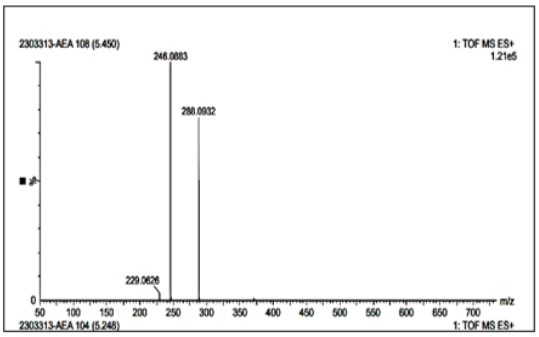
IR Spectrum of Compound EPNB-07 (Luteolin)



^{1}HNMR Spectrum of (Luteolin)

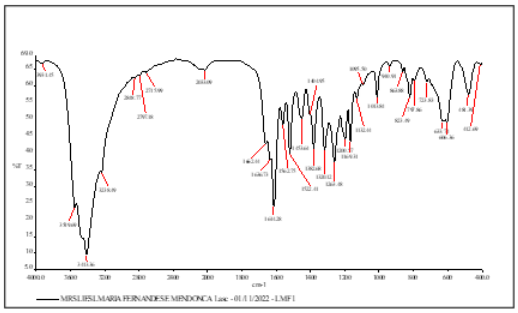


^{13}CNMR Spectrum of (Luteolin)

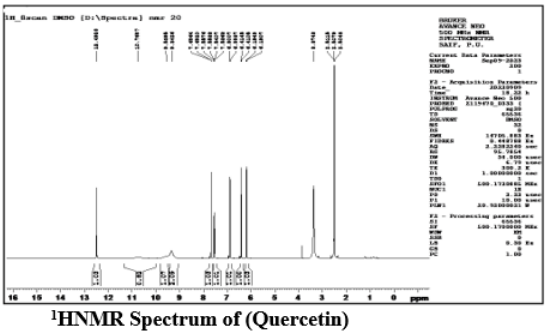


Mass Spectrum of (Luteolin)

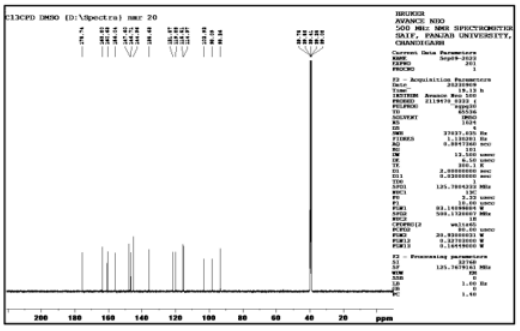
EPNB-08



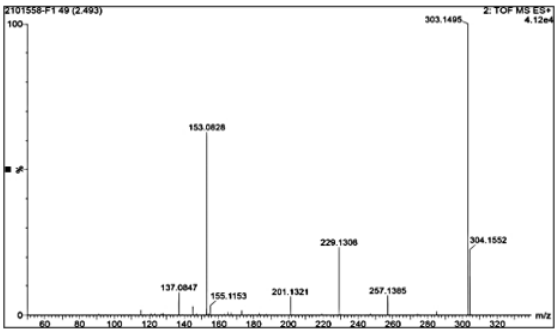
IR Spectrum of Compound EPNB-08 (Quercetin)



^{1}HNMR Spectrum of (Quercetin)

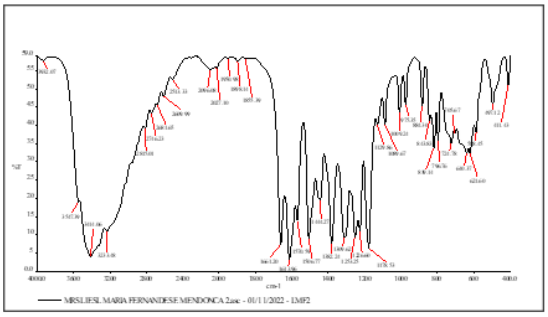


^{13}CNMR Spectrum of (Quercetin)

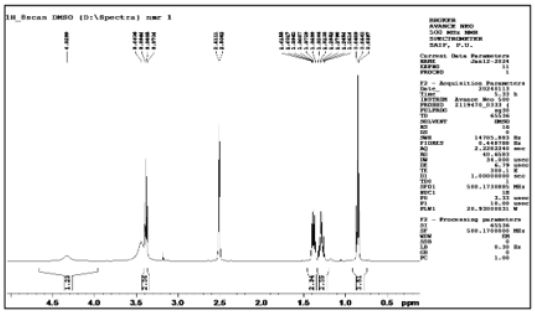


Mass Spectrum of (Quercetin)

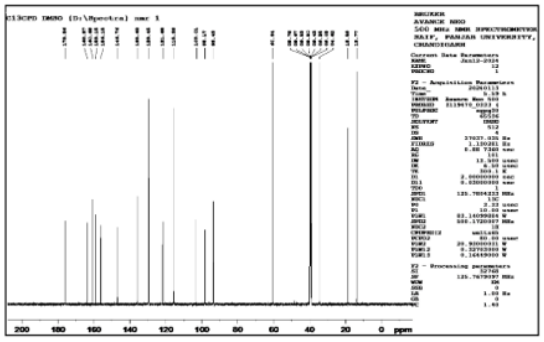
EPNB-09



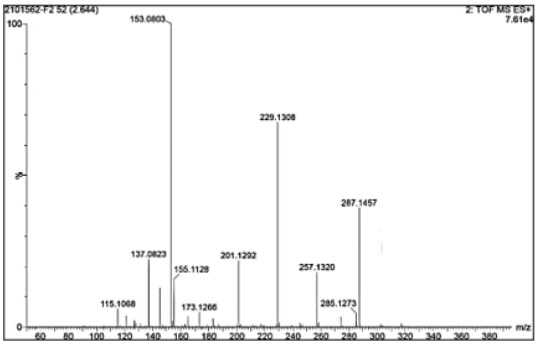
IR Spectrum of Compound EPNB-09 (Kaempferol)



^{1}HNMR Spectrum of (Kaempferol)



^{13}CNMR Spectrum of (Kaempferol)



Mass Spectrum of (Kaempferol)